4

Binary Metal-Organic Frameworks

4.1 Introduction

In Chapter 3 we have explored the wide range of linker shapes accessible through organic synthesis and gave an insight into the chemistry of the secondary building units (SBUs), the elements they are typically composed of, and their variety with respect to geometry and connectivity. Combining these two components allows for the formation of a myriad of extended framework structures with different topologies. In this chapter, we will analyze important framework structures categorized by the connectivity of their SBUs starting from low connectivity and work our way up to highly connected SBUs.

4.2 MOFs Built from 3-, 4-, and 6-Connected SBUs

4.2.1 3-Connected (3-c) SBUs

Most structures based on 3-connected (3-c) nets are found in coordination networks built from single metal nodes and neutral donor linkers. In contrast, the 3-c species in metal-organic framework (MOF) structures is most often the organic linker. However, there are examples of MOF structures involving 3-c SBUs, such as the dinuclear paddle wheel $M_2(–COO)_3$ (e.g. M = Cu^{2+}, Zn^{2+}), an SBU that is closely related to the more common 4-c paddle wheel $M_2(–COO)_4$ we encountered earlier. As discussed in Chapter 3, subtle changes in the reaction conditions can have a dramatic impact on which SBU forms and thus also on the structure of the resulting MOF. An example of this is PNMOF-3 ($Zn_4(NH_2\text{-BDC})_3(NO_3)_2(H_2O)_2$). Even though PNMOF-3 is synthesized from the very same starting materials ($Zn(NO_3)_2$ and (NH_2)-H_2BDC) as IRMOF-3 ($Zn_4O(NH_2\text{-BDC})_3$) its structure is fundamentally different [1]. PNMOF-3 comprises 3-c $Zn_2(–COO)_3$ paddle wheel SBUs rather than the 6-c octahedral $Zn_4O(–COO)_6$ SBUs found in IRMOF-3 and the formation of these 3-c paddle wheel SBUs is ascribed to the presence of a cross-linked copolymer in the reaction mixture, hence the name PNMOF-3. The hexagonal crystal structure of PNMOF-3 consists of stacked 2D layers of **hcb** (honeycomb) topology (Figure 4.1) that are stacked in an eclipsed arrangement resulting in hexagonal channels of 14.9 Å diameter running along the crystallographic *c*-axis. The

Introduction to Reticular Chemistry: Metal-Organic Frameworks and Covalent Organic Frameworks,
First Edition. Omar M. Yaghi, Markus J. Kalmutzki, and Christian S. Diercks.

Companion website: www.wiley.com/go/yaghi/reticular

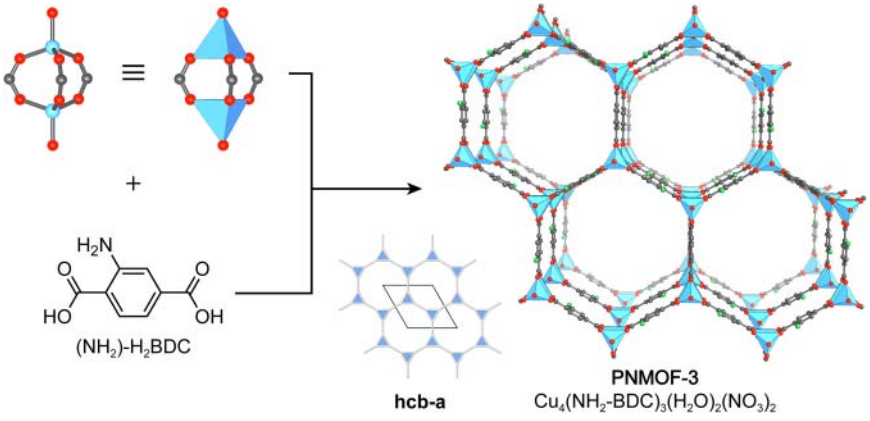

Figure 4.1 Crystal structure of PNMOF-3 formed by reticulation of Zn^{2+} and (NH_2)-H_2BDC in the presence of a cross-linked copolymer. The reticulation of a 3-c SBU and ditopic (NH_2)-H_2BDC linkers affords a framework of **hcb** topology. The eclipsed arrangement of the hexagonal layers leads to the formation of hexagonal channels of 14.9 Å. All hydrogen atoms are omitted for clarity. Color code: Cu, blue; C, gray; N, green; O, red.

charge of the cationic framework is compensated by one terminal nitrate ligand per $Zn_2(–COO)_3$ paddle wheel SBU. Even though the 3-c dinuclear paddle wheel SBU is less common than its 4-c analog ($Zn_2(–COO)_4$), several highly stable porous frameworks based on this SBU are known [2].

4.2.2 4-Connected (4-c) SBUs

The most common 4-connected (4-c) SBU in MOF chemistry is the dinuclear paddle wheel $M_2(–COO)_4$ (e.g. M = Cu^{2+}, Zn^{2+}, Co^{2+}), in which each metal ion is coordinated in a square-pyramidal fashion by four oxygen of the bridging carboxylates and one terminal neutral ligand, most often water. For clarity, the capping ligands are often omitted, and the paddle wheel unit is represented as two squares connected by four carboxylates. In terms of net topology, the paddle wheel is represented by a square 4-c vertex figure (Figure 4.2).

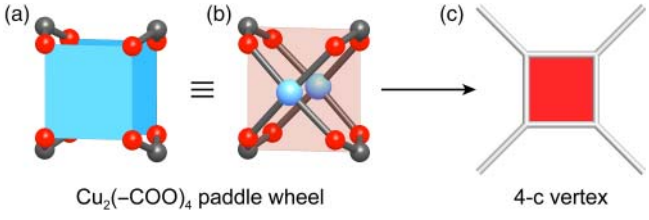

Figure 4.2 Representations of the dinuclear $M_2(–COO)_4$ paddle wheel SBU. (a) Two metal centers form a dinuclear paddle wheel complex. (b) Connecting the carboxylate carbons reduces the paddle wheel to a square building unit with four points of extension. (c) Topological representation of the vertex figure as a 4-c square building unit. Color code: Cu, blue; C, gray; O, red.

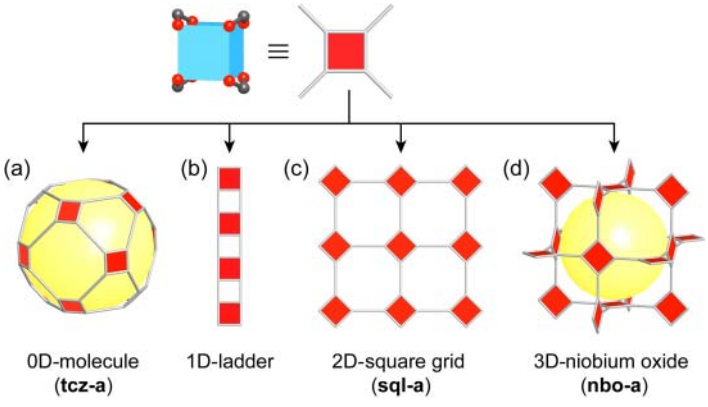

Figure 4.3 Topologies of structures formed by linking 4-c paddle wheel SBUs (represented by red squares) and ditopic linkers (gray lines connecting the squares). The precise geometry of the linker directs the reticular synthesis toward (a) discrete, 0D metal-organic polyhedra (MOPs, here a truncated cuboctahedron [**tcz-a**] is shown), (b) 1D chain/ladder, (c) 2D square layers (**sql-a** or **fes**), and (d) 3D networks (here a niobium oxide net [**nbo-a**] is shown). In the case of the **nbo** net, the yellow ball is placed in the frame of the structure as a visual aid. Note that all ditopic linkers are represented by gray lines regardless of their exact molecular structure.

Linking such 4-c square building units with ditopic linkers can afford a variety of different structures depending on the exact geometry of the linker. Here, we will discuss the geometrical requirement for the formation of (i) discrete 0D metal-organic polyhedra (MOPs)[1], (ii) 1D chains, (iii) 2D layers, and (iv) 3D networks (Figure 4.3).

While the geometry of the paddle wheel SBU is fixed, in the molecular structure of ditopic linkers, three different angles can be deliberately modified: a bending angle θ between the coplanar binding groups can be introduced by altering the positions of the binding groups on the central unit, a dihedral angle φ between the binding groups is created by twisting them about the axis of the linker, and an angle ψ between the planes of the binding groups results from bending them toward each other (Figure 4.4).

Reticulating Cu^{2+} ions and ditopic *m*-H_2BDC linkers with a bending angle θ of approximately 120° between the coplanar carboxylic binding groups yields a 0D MOP of **tcz** topology, called MOP-1 (Cu_2(*m*-BDC)$_2$, Figure 4.5) [3]. MOPs of the same topology can generally be synthesized by reticulating ditopic linkers that have an angle θ between 90° and 120° with metal ions favoring the formation of square 4-c paddle wheel SBUs. The synthesis and design of MOPs is part of reticular chemistry and is further discussed in Chapter 19. Examples illustrating the use of MOPs as tertiary building units (TBUs) in the synthesis of extended structures are discussed in Chapter 5.

Introduction of an angle ψ between the two carboxylate binding groups of the linker, as in 4,4′-DMEDBA, and reticulation of this linker with Cu^{2+}

1 MOPs will be discussed in more detail in Chapter 19.

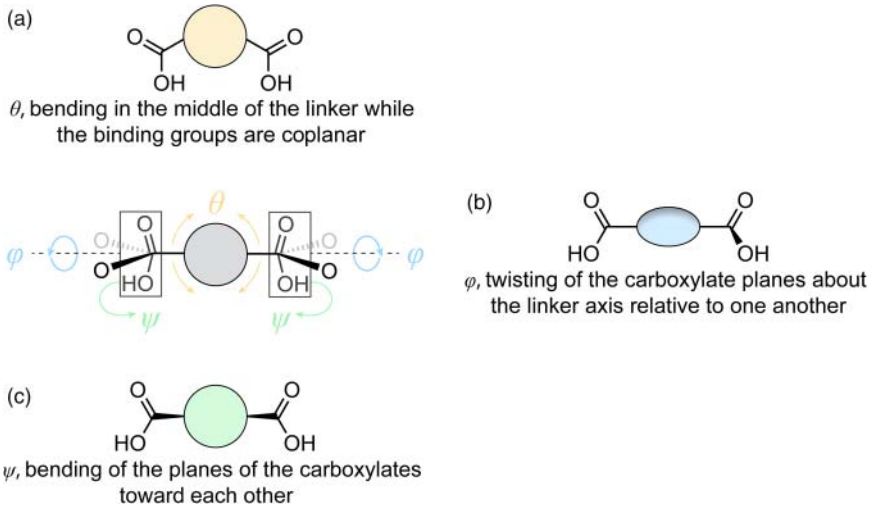

Figure 4.4 Different angles on a ditopic linker that can be altered by precise design of the molecular structure. (a) The bending angle θ refers to a bent linker with coplanar binding groups, (b) the dihedral angle φ refers to non-coplanar binding groups, and (c) the angle ψ refers to binding groups bent toward each other.

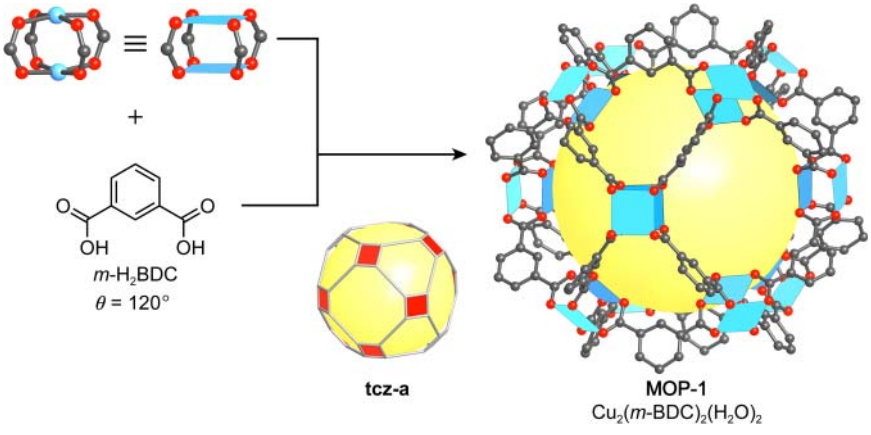

Figure 4.5 Reticulation of m-H_2BDC and Cu^{2+} ions facilitates the formation of a molecular polyhedron of **tcz**, termed MOP-1. Here, the precise adjustment of θ, the bending angle between the coplanar binding groups, dictates the product of the synthesis. The terminal water ligands on the copper paddle wheel as well as all hydrogen atoms are omitted for clarity. The yellow sphere represents the empty space within the **tcz** polyhedron. Color code: Cu, blue; C, gray; O, red.

gives MOF-222 (Cu_2(4,4′-DMEDBA)$_2$) with a structure built from 1D chains (Figure 4.6) [4].

A 2D structure is formed when 4-c copper paddle wheel SBUs are connected by linear ditopic linkers with coplanar carboxylic acid binding groups ($\varphi = 180°$). In this scenario, the binding groups are either coplanar to the backbone of the

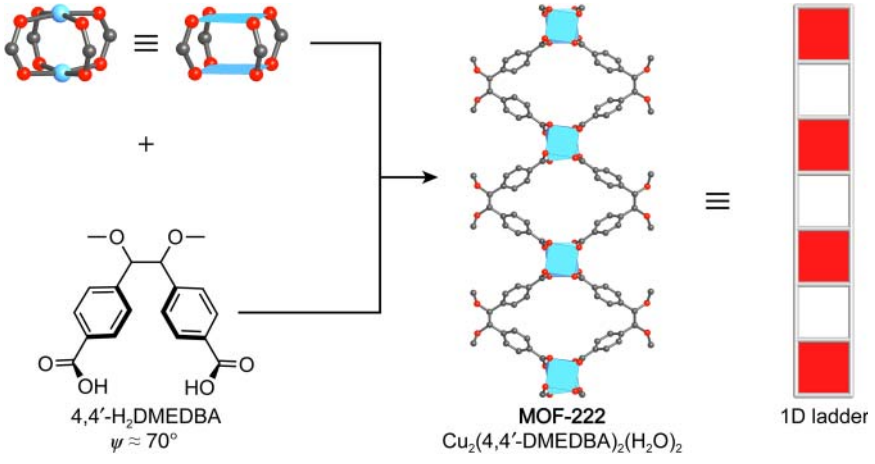

Figure 4.6 Crystal structure of MOF-222. The formation of 1D chains by linking 4-c paddle wheels and ditopic linkers is achieved by introducing an angle ψ (approximately 70°) between the two carboxylate binding groups. The terminal water ligands on the copper paddle wheel SBUs as well as all hydrogen atoms are omitted for clarity. Only a section of one chain is shown. Color code: Cu, blue; C, gray; O, red.

linker, as in the case of the H_2BDC (MOF-2, see Figure 1.14), or they are rotated out of plane with respect to the central aryl unit, as in the case of (Cl_2)-H_2BDC (Figure 4.7). The steric hindrance of the chlorine substituents increases the rotational barrier, thereby fixing the binding groups in a coplanar orientation perpendicular to the aryl core unit. Joining 4-c paddle wheel SBUs through BDC or (Cl_2)-BDC affords 2D **sql** structures termed MOF-2 and MOF-102 ($Cu_2(Cl_2$-BDC$)_2$), respectively (Figure 4.7) [5].

A combination of ditopic linkers and 4-c paddle wheel units can further be used to construct extended 3D frameworks. This is achieved when a dihedral angle ($\varphi \neq 0°$) between the two binding groups of the ditopic linker is introduced, resulting in MOFs with **nbo** (niobium oxide) topology as exemplified by MOF-101 (Cu_2(*o*-Br-BDC$)_2$) illustrated in Figure 4.8 [6]. In this example, the sterically demanding bromide substituent on the linker increases the rotational barrier of one of the carboxylic acid groups, fixing the binding groups in a perpendicular orientation with respect to each other. While the synthesis at low temperatures affords MOF-101, at elevated temperatures, where the rotational barrier can be overcome by thermal energy, a framework of **sql** topology is formed.

The above shown examples illustrate the importance of the precise geometrical design of the molecular structure of linker molecules to direct the synthesis into either 0D, 1D, 2D, or 3D structures. The example of MOF-101 also highlights that it is important to adjust the reaction conditions to ensure an unaltered linker geometry throughout the reticulation process. These considerations emphasize that careful analysis of the geometry of the building units as well as their physical and chemical properties is required to enable the *a priori* synthesis of MOFs [7].[2]

2 Further examples on linking up squares are reported in a 2002 review article [5].

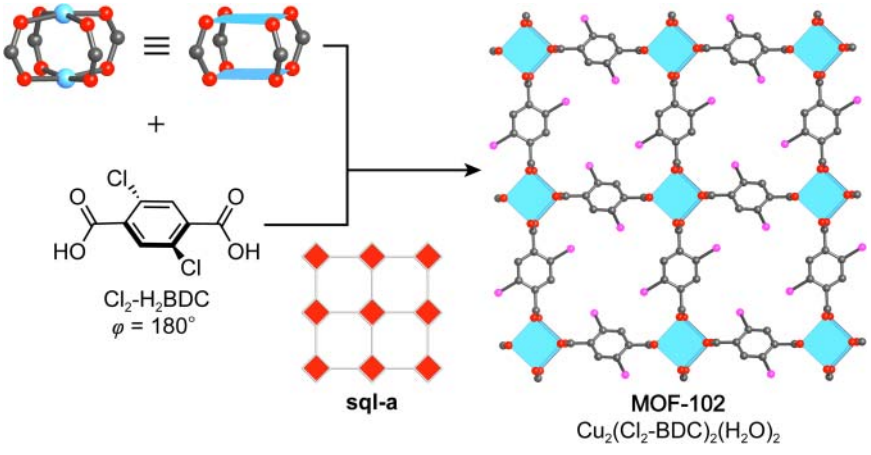

Figure 4.7 Crystal structure of MOF-102. The combination of 4-c square SBUs and linear ditopic linkers with coplanar binding groups ($\varphi = 180°$) leads to the formation of a 2D framework with **sql** topology. The **sql** layers are stacked along the *c*-direction, here, only one layer is shown for clarity. The terminal water ligands on the copper paddle wheel SBUs as well as all hydrogen atoms are omitted for clarity. Color code: Cu, blue; C, gray; O, red; Cl, pink.

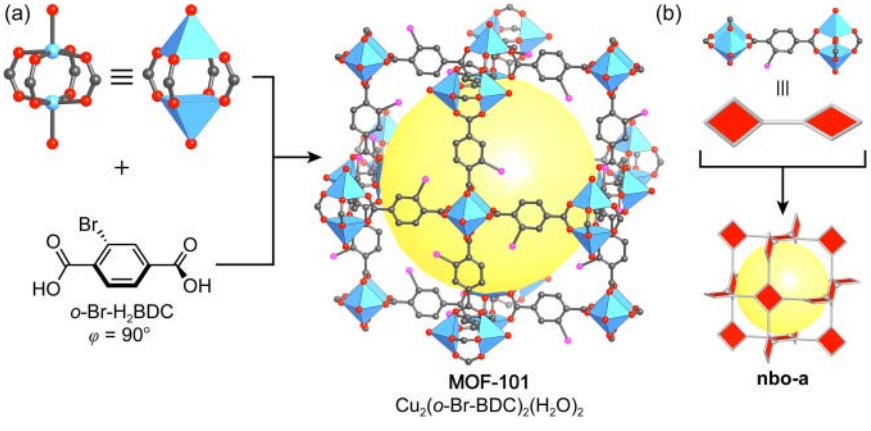

Figure 4.8 (a) The cubic crystal structure of MOF-101 formed by reticulation of 4-c copper paddle wheel SBUs and linear ditopic *o*-Br-H$_2$BDC linkers. (b) The structure has an underlying **nbo** topology. The formation of this net is achieved by introducing a dihedral angle ($\varphi = 90°$) between the two binding groups. All hydrogen atoms are omitted for clarity. Color code: Cu, blue; C, gray; O, red; Br, pink.

Another way to form 3D frameworks using 4-c paddle wheel SBUs is to use organic linkers with more than two points of extension. An early example of this approach is HKUST-1 (HKUST = Hong Kong University of Science and Technology) ($Cu_3(BTC)_2$, BTC = benzenetricarboxylate), a MOF based on a 3,4-connected **tbo** (twisted boracite) net (Figure 4.9) [8]. The structure comprises 4-c copper paddle wheel SBUs and tritopic BTC linkers, and encompasses an

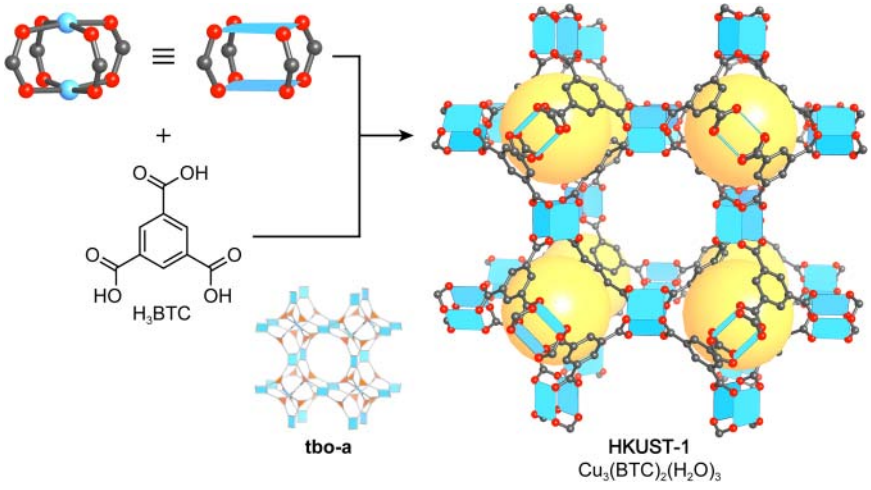

Figure 4.9 Crystal structure of HKUST-1. The **tbo** net is formed by linking 4-c $Cu_2(–COO)_4$ SBUs with trigonal tritopic BTC linkers (D_{3h} symmetry). Each large cubic pore is surrounded by four smaller octahedral pores. The large pores are connected through square windows and form a 3D intersecting pore system. The inset shows the augmented **tbo-a** net. The terminal water ligands on the copper paddle wheel SBUs and all hydrogen atoms are omitted for clarity. Color code: Cu, blue; C, gray; O, red.

intersecting 3D system with square pore openings of 9 × 9 Å. The overall void space is 40.7%, a value comparable to that of many zeolites.

The terminal water ligands bound axially to the paddle wheel SBUs in HKUST-1 can be removed by heating in dynamic vacuum, which results in open metal sites and a color change of the material from blue to purple. Initial gas adsorption measurements yielded relatively low surface areas since the MOF was not properly activated, more recent measurements gave surface areas of up to 2200 $m^2\ g^{-1}$. The high density of open metal sites in fully activated HKUST-1 makes it one of the best performing materials with respect to natural gas and hydrogen storage [9]. HKUST-1 structures containing metals other than copper are architecturally unstable and collapse upon activation as evidenced by the observed negligible nitrogen uptake [10]. The modular structure of HKUST-1 initiated the development of many isoreticular expanded versions such as PCN-6 (PCN = Porous Coordination Network) or MOF-399 [11]. The latter still holds the world record for the lowest density MOF (0.126 g cm^{-3}).

The H_3BTC linker employed in the synthesis of HKUST-1 has D_{3h} symmetry, with all carboxylic acid groups being coplanar to the central aryl unit. As discussed earlier, the precise geometry of the linker dictates whether a specific topology is favored over another. Hence, when an expanded version of H_3BTC is designed it is required that the overall planar conformation is retained. Symmetric elongation of H_3BTC by one benzene ring gives H_3BTB. Here, the steric repulsion between the aromatic protons of the central aryl unit and those of the terminal benzoic acid groups enforces a dihedral angle between them causing

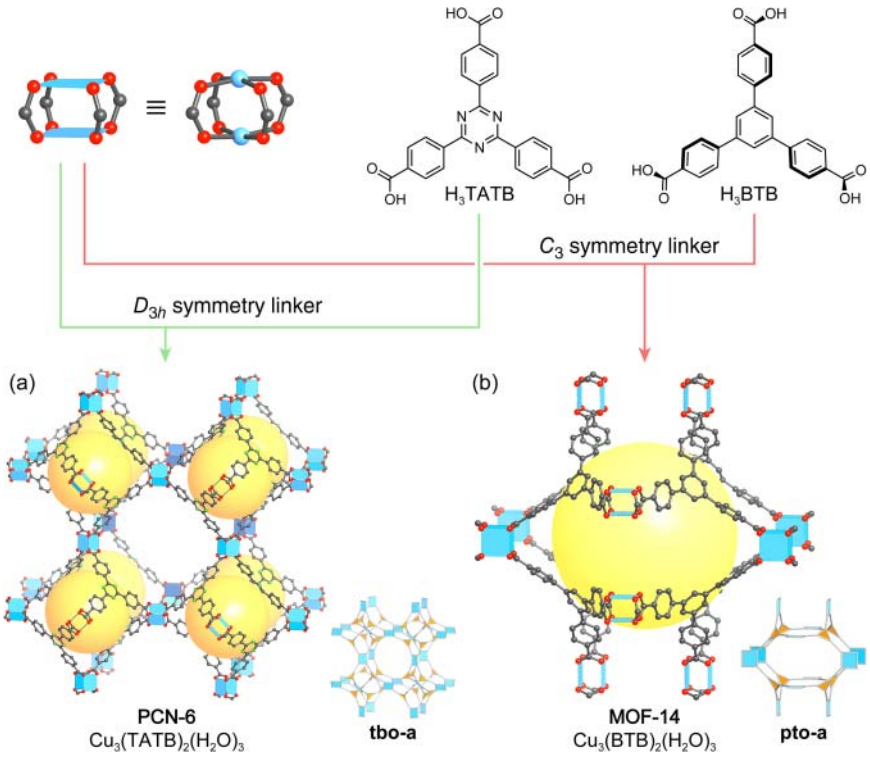

Figure 4.10 Comparison of the crystal structures of PCN-6 and MOF-14. Both structures represent 3,4-connected nets. (a) The D_{3h} symmetry of the H_3TATB linker affords the formation PCN-6 (**tbo**), (b) whereas the lower C_3 symmetry of H_3BTB directs the synthesis toward the formation of MOF-14 (**pto**). Terminal water ligands on the copper paddle wheel SBUs, all hydrogen atoms, and all interpenetrating frameworks in the structure of MOF-14 are omitted for clarity. Color code: Cu, blue; C, gray; N, green; O, red.

H_3BTB to have C_3 (propeller shape) instead of D_{3h} symmetry. Therefore, the reticulation of H_3BTB and Cu^{2+} cannot afford a framework of **tbo** topology and consequently the formation of an interpenetrated framework of **pto** (platinum oxide) topology, termed MOF-14 ($Cu_3(BTB)_2$), is favored (Figure 4.10b) [12]. Despite interpenetration, MOF-14 has large cavities of 16.4 Å diameter and a pore aperture of 7.66×14 Å. To avoid the nonplanar conformation of the linker due to steric repulsion between the aromatic protons a triazine core unit can be used. In this way, the perfectly planar expanded equilateral tritopic linker H_3TATB (D_{3h} symmetry) can be synthesized, which allows for the formation of a framework with an underlying **tbo** topology, termed PCN-6 ($Cu_3(TATB)_2$) (Figure 4.10) [13].

4.2.3 6-Connected (6-c) SBUs

6-c SBUs can be built from a wide range of metals and can have different geometries ranging from highly symmetric octahedral, trigonal prismatic, and hexagonal planar, to lower more distorted symmetries. Here we will discuss

the most frequently encountered 6-c SBUs in MOF chemistry and important structures built therefrom.

The octahedral $Zn_4O(–COO)_6$ SBU is one of the most common building units in MOF chemistry. In Chapter 2 we have discussed the structures of MOF-177 and its isoreticular expanded analogs having the **qom** topology (hetero-dual, highest symmetry embedding $P\bar{3}1c$, No. 159).[3] Because the **qom** topology is not the default topology for the combination of trigonal and an octahedral building units, frameworks built from a combination of these building units are expected to crystallize in the higher symmetry 3,6-connected **pyr** topology (self-dual, highest symmetry embedding $Pa\bar{3}$, No. 205). While the **qom** net is a hetero-dual net, and structures of this topology are thus not expected to interpenetrate upon isoreticular expansion of **pyr** frameworks (self-dual net) results in interpenetrated frameworks. Here, we want to compare two related structures, MOF-150 ($Zn_4O(TCA)_2$) and MOF-177 ($Zn_4O(BTB)_2$) with underlying **pyr** and **qom** topology, respectively, and present possible factors leading to the formation of one topology or the other (Figure 4.11). Since the synthesis conditions for both MOFs are similar, no structure directing agent is employed, and the SBUs in both compounds are identical, the formation of the two different topologies must originate from the linkers. Both MOFs are built from equilateral trigonal tritopic linkers with terminal benzoic acid groups that only differ in their respective core unit. The H_3TCA linker employed to prepare MOF-150 is constructed around a monoatomic nitrogen core that facilitates the free and independent rotation of the three terminal benzoate units. In contrast, due to steric repulsion between aromatic hydrogen atoms within the H_3BTB linker used in the synthesis of MOF-177, more constraints are imparted with respect to the dihedral angle between the aryl core and the terminal benzoic acids, and their orientation relative toward each other. Linking basic zinc carboxylate SBUs and BTB gives a framework of **qom** topology, whereas the reticulation of the same SBU and TCA linkers directs the framework formation toward the higher symmetry **pyr** topology. Here, the edge-transitive **pyr** net is the thermodynamic and the **qom** net is the kinetic product.

With more than 400 reported MOF structures, trigonal prismatic SBUs of the general formula $M_3OL_3(–COO)_6$ ($M = Al^{3+}$, In^{3+}, Cr^{3+}, V^{3+}) are among the most common inorganic building units of MOFs [14]. A structurally similar SBU of general formula $M_3(–COO)_6$ can be formed from divalent metals such as copper. In the following text, we will discuss some examples of MOFs constructed from the $M_3OL_3(–COO)_6$ SBU and linear ditopic (MIL-101), trigonal tritopic (MIL-100), and rectangular tetratopic (**soc**-MOF) linkers [14c, d, f, g].

Both, MIL-100 ($[M_3OL_3](BTC)_2$) and MIL-101 ($[M_3OL_3](BDC)_3$) (MIL = Materials Institute Lavoisier), are built from trigonal prismatic $M_3OL_3(–COO)_6$ SBUs and share the same topology even though the linker used in their synthesis are of different topocity; tritopic H_3BTC is used to prepare MIL-100 and ditopic H_2BDC is employed in the synthesis of MIL-101 [14b–d]. This may seem confusing at first but can be explained in terms of choosing larger

3 For more information on the terminology used in the topological description of crystal structures see Chapter 18.

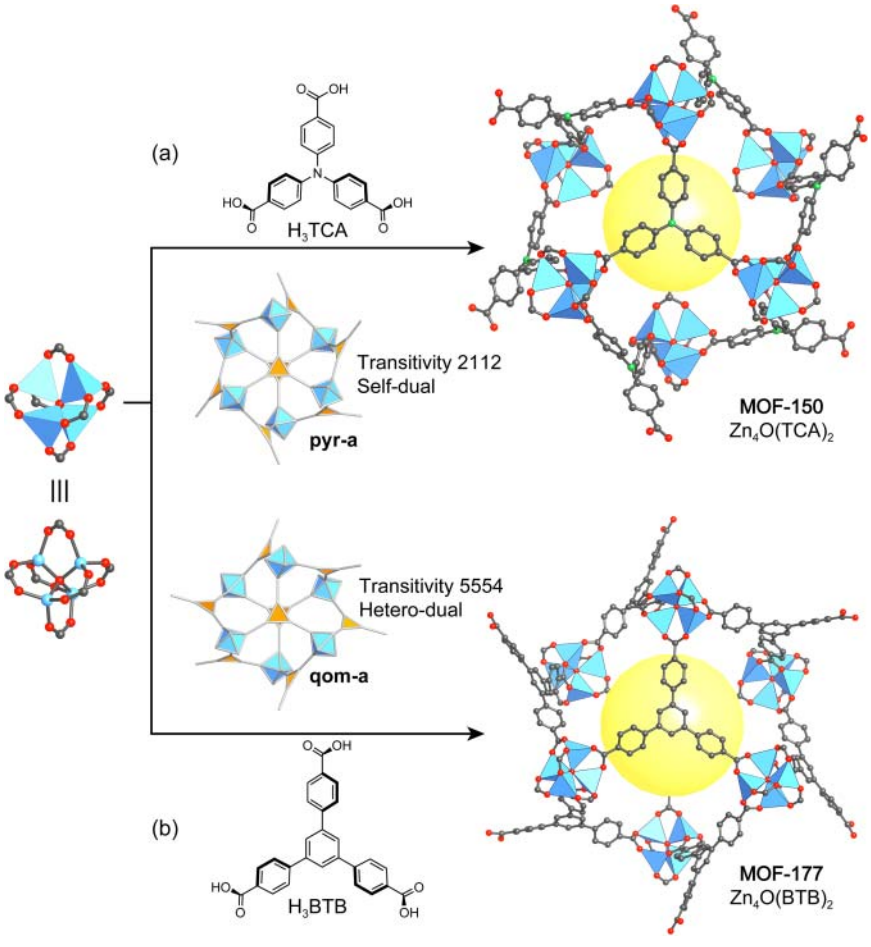

Figure 4.11 Comparison of the crystal structures and topologies of MOF-150 and MOF-177. (a) A framework with the default self-dual **pyr** net (transitivity 2112) is formed when H_3TCA is used, (b) while employing H_3BTB affords the formation of a framework based on the **qom** net (transitivity 5554), a hetero-dual net that is unlikely to support interpenetration. The corresponding augmented nets are shown next to the respective crystal structure. All hydrogen atoms are omitted for clarity. Color code: Cu, blue; C, gray; N, green; O, red.

"tertiary building units" rather than secondary building units to simplify the overall structure. In the case of MIL-100 and MIL-101, these TBUs are tetrahedral units formed by linking four 6-c SBUs by either four BTC or six BDC units (Figure 4.12, top). In MIL-100 the tritopic BTC linker is positioned on the faces of these tetrahedra, whereas in MIL-101 the ditopic linkers constitute their edges (Figure 4.12). By further linking these tetrahedral TBUs in a vertex-sharing manner two differently sized cages are formed that are connected through 5-membered rings to give a framework with an overall **mtn** topology, a tetrahedral topology commonly found in zeolites (Figure 4.12, bottom) [15].

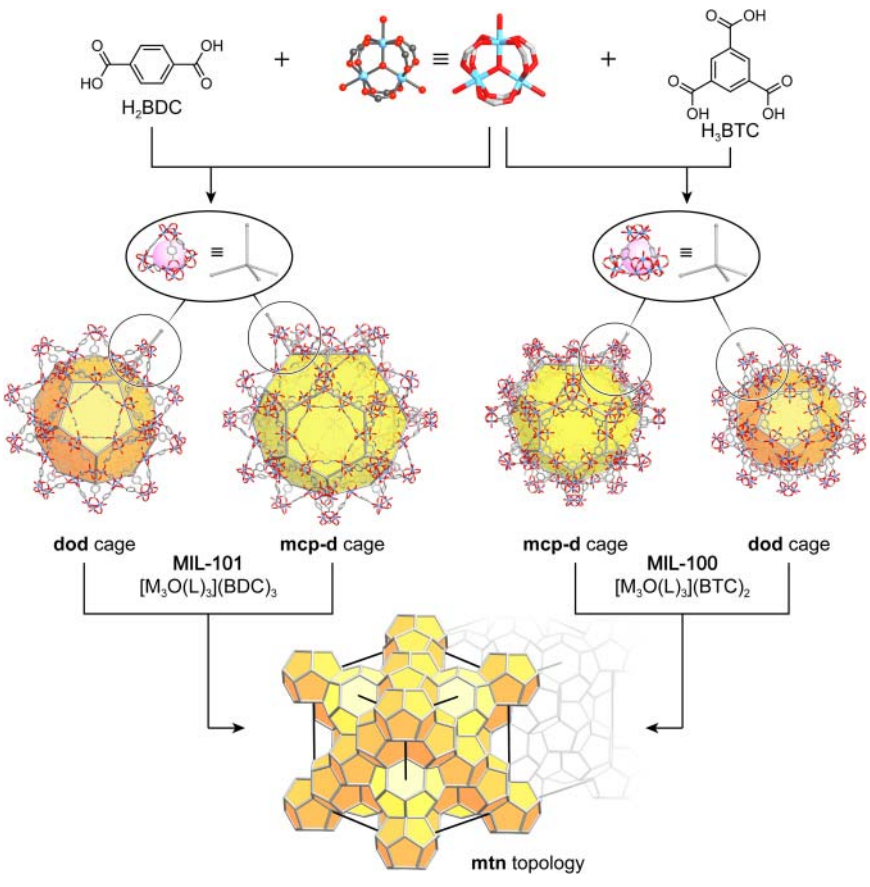

Figure 4.12 Topological analysis of the structures of MIL-100 and MIL-101. In both structures, tetrahedral TBUs are formed by joining trinuclear $M_3OL_3(–COO)_6$ SBUs with trigonal tritopic BTC or linear ditopic BDC linkers, respectively. These TBUs are further linked to form two differently sized cages (a small **dod** and a large **mcp-d** cage) that are fused to give frameworks of **mtn** topology. All hydrogen atoms are omitted for clarity. Color code: Metal, blue; C, gray, O, red; **dod** cages are represented as orange, **mcp-d** cages as yellow polyhedra.

In MIL-100 these cages have diameters of 25 and 29 Å with pore openings of 5 and 9 Å, respectively [14c]. With diameters of 29 and 34 Å and pore openings of 12 and 16 Å, the cages in MIL-101 are slightly larger [14d]. Both materials displayed unprecedented chemical stability at the time of their discovery, which in combination with their zeolite-like structure (small pore apertures, large cages) made them interesting candidates for their application in catalytic processes. Accordingly, the incorporation of functional groups, discrete molecules, and metal nanoparticles into the pores of MIL-101 was pursued. The resulting materials typically show high catalytic activities for a variety of organic transformations [14e, 16]. The expansion of the linkers used in the synthesis of MIL-100 and MIL-101 yields an isoreticular series of frameworks with pore sizes up to 68 Å (see Figure 2.13) [17].

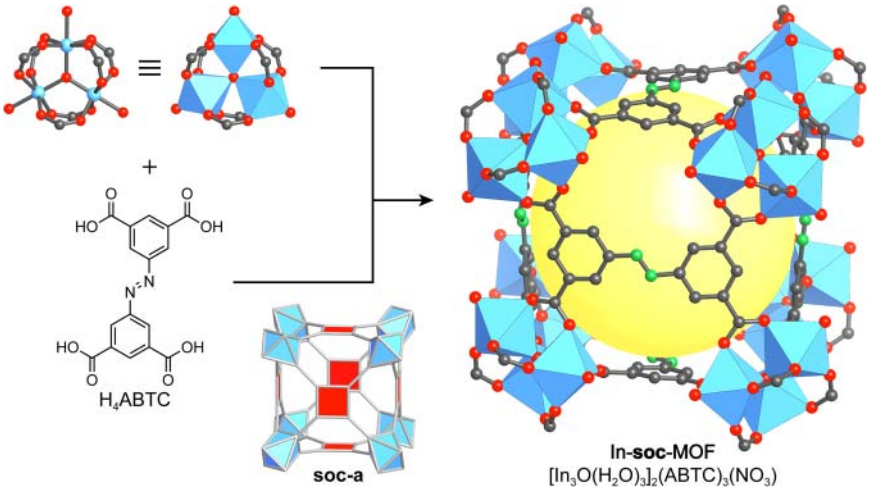

Figure 4.13 Crystal structure of In-**soc**-MOF and its topology representation as a **soc** net. Removal of the terminal water ligands affords the creation of open metal sites pointing into the narrow pores. The augmented **soc** net is depicted next to the crystal structure of In-s**oc**-MOF. The NO_3 counter ions residing in the open pores of the framework as well as all hydrogen atoms are omitted for clarity. Color code: In, blue; C, gray; N, green; O, red.

MOFs with an underlying 4,6-connected **soc**[4] topology are another important example of framework structures involving $M_3OL_3(-COO)_6$ SBUs. The structure of In-**soc**-MOF ($[In_3O(H_2O)_3]_2(ABDC)_3NO_3$) is built from rectangular offset tetratopic ABTC linkers and trigonal prismatic $In_3O(H_2O)_3(-COO)_6$ SBUs (Figure 4.13). The chemical formula of the SBU suggests a cationic framework where the charge is neutralized by $(NO_3)^-$ anions residing in the pores of the open framework structure [14f]. The crystal structure of In-**soc**-MOF and the underlying **soc** topology are given in Figure 4.13.

The terminal water ligands on the $In_3O(H_2O)_3(-COO)_6$ SBUs can be removed by activation under dynamic vacuum at elevated temperatures, leaving behind open metal sites pointing into the narrow pores of the MOF. This results in a high localized charge density within the pores that is advantageous for gas adsorption, in particular for hydrogen storage. This is indeed the case for In-**soc**-MOF, which has a comparatively high hydrogen storage capacity of 2.61% at 78 K and 1.2 atm. As expected, H_2 is strongly bound to the open metal sites (primary adsorption site) and at higher loadings, other adsorption sites with lower binding energy are occupied as evidenced by inelastic neutron scattering experiments [14f]. MOFs with the same underlying topology, but built from a lighter metal, hold great promise with respect to gas storage applications, since an increase in gravimetric gas uptake is expected while the high volumetric uptake is retained. This principle is used in the construction of an isoreticular

4 The denotation **soc**, or "square-octahedron" refers to the reticulation of square and octahedral building units.

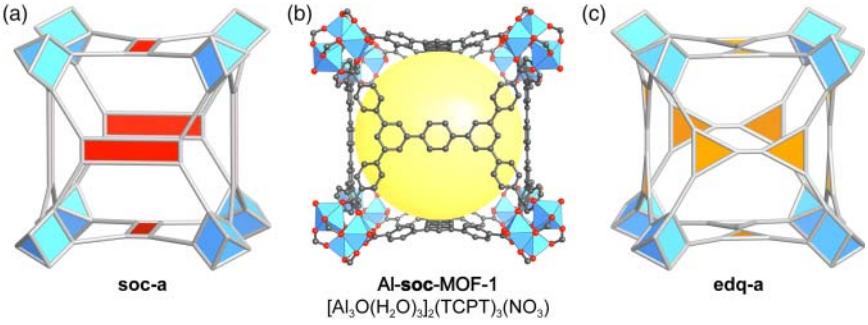

Figure 4.14 Comparison of the structure of Al-**soc**-MOF and the **soc** and **edq** topology. (b) Unit cell of Al-**soc**-MOF-1. The framework is built from trigonal prismatic $Al_3OL_3(–COO)_6$ SBUs that are linked by TCPT moieties. (a, c) The structure can be deconstructed into the **soc** or the **edq** topology. In the **soc** net the linker is represented as one tetratopic building unit (left), and as two linked trigonal tritopic building units in the **edq** net (right). Color code: Al, blue; C, gray; O, red.

series of highly porous aluminum-based **soc**-MOFs. The Al-**soc**-MOF platform meets the challenging Department of Energy (DOE) dual target for methane storage of $0.5\,g\,g^{-1}$ (gravimetric) and $264\,cm^3\ cm^{-3}$ (volumetric) [14g]. The structure of Al-**soc**-MOF-1 ($[In_3O(H_2O)_3]_2(TCPT)_3(NO_3)$) is illustrated in Figure 4.14. From a topological point of view the tetratopic rectangular linker applied in the synthesis of all **soc**-MOFs can also be described as two triangular vertex figures that are connected by an edge and thus the Al-**soc**-MOF can also be described by the 3,6-connected **edq** net. Both descriptions are acceptable, and it is the chemical backbone of the organic linker that makes one or the other the more plausible choice (Figure 4.14).

The chemistry of zirconium carboxylates, especially that of $Zr_6(\mu_3\text{-}O)_4(\mu_3\text{-}OH)_4(RCOO)_{12}$ clusters, is well established in molecular inorganic chemistry and SBUs with an analogous structure are known in MOF chemistry. Such SBUs are based on the same Zr_6O_8-core and, in contrast to their molecular analogs, they can have a connectivity ranging between 6 and 12 [18]. This is because not all carboxylates have to originate from linkers connecting the SBUs, but monofunctional carboxylic acids or –OH and $–OH_2$ moieties can act as terminal ligands.

For a 6-c SBU based on the Zr_6O_8-core, two distinct geometries can be envisioned: trigonal antiprismatic and hexagonal planar (Figure 4.15). Both geometries have been found in frameworks involving trigonal tritopic linkers. Which of these two geometries is adopted in a given framework strongly depends on the exact geometry of the linker as well as the reaction conditions, in particular the amount and nature of modulator employed in the synthesis. Modulators are additives that influence the rate of formation of the SBU and the framework, and therefore the crystallinity of the resulting MOF. Among the most common modulators in carboxylate MOF chemistry are organic monocarboxylic acids (e.g. formic, acetic, benzoic acid) or inorganic acids (e.g. HCl, HNO_3).

Reticulating Zr^{4+} ions and H_3BTC linkers (D_{3h} symmetry) leads to the formation of trigonal antiprismatic SBUs that are linked by BTC units to form

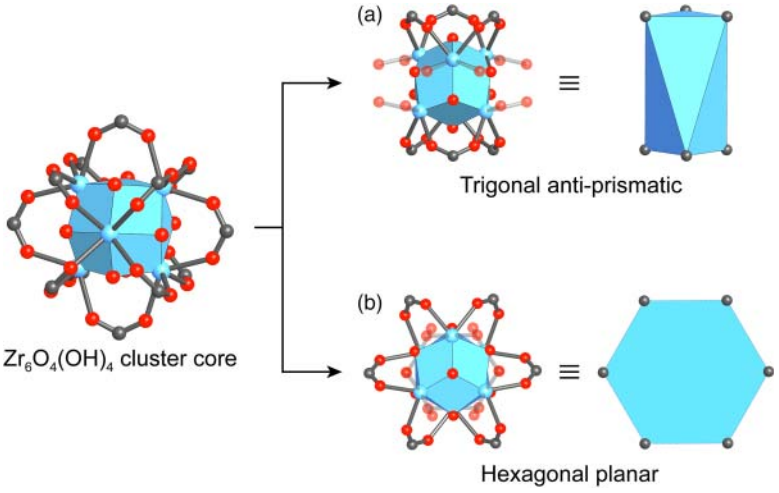

Figure 4.15 SBUs based on the Zr_6O_8-core can have up to 12 points of extension. For a 6-c version, two geometries are possible: (a) trigonal antiprismatic and (b) hexagonal planar. Which of these SBUs forms depends on the precise geometry of the linker. Color code: Zr, blue; C, gray; O, red.

a crystalline framework termed MOF-808 ($Zr_6O_4(OH)_4(HCOO)_6(BTC)_2$) with an overall **spn** topology, the default topology for the combination of trigonal and trigonal antiprismatic building units [19]. The trigonal antiprismatic $[Zr_6(\mu_3\text{-}O)_4(\mu_3\text{-}OH)_4]^{12+}$ core of the SBUs is connected to six BTC linkers and the remaining uncoordinated metal sites are occupied by formate ligands. Each BTC linker is connected to three neighboring trigonal anti-prismatic SBUs to form tetrahedral subunits with an internal pore diameter of 4.8 Å. These tetrahedral units are further linked in a vertex-sharing manner to give adamantane-like cages with a pore diameter of 18.4 Å. The structure can be described by either the **spn** topology (6-c trigonal anti-prismatic and 3-c trigonal building units) or, alternatively a **dia** topology, where larger tetrahedral TBUs are defined (Figure 4.16).

As discussed earlier in this chapter expanded analogs of the H_3BTC linker employed in the synthesis of MOF-808 can be prepared. Replacing the three terminal carboxylic acid binding groups by benzoic acid groups is accompanied by a decrease in symmetry (H_3BTB has C_3 rather than D_{3h} symmetry). This distortion can be circumvented by using a triazine core unit as in the case of H_3TATB (D_{3h} symmetry). Consequently, using the H_3TATB linker it is possible to prepare an isoreticular expanded version of MOF-808 termed PCN-777 ($Zr_6O_4(OH)_4(HCOO)_6(TATB)_2$), whereas a MOF with a different topology is formed when the nonplanar H_3BTB linker is used. The fact that the carboxylic acid binding groups in H_3BTB are not coplanar with respect to each other prevents the formation of an **spn** topology framework [20]. Hence, the resulting MOF (UMCM-309a, UMCM = University of Michigan Crystalline Material, $Zr_6O_4(OH)_4(BTB)_6(OH)_6(H_2O)_6$) has a 2D layered structure with a **kgd** (kagome dual) instead of the default **spn** topology [21]. In the structure of

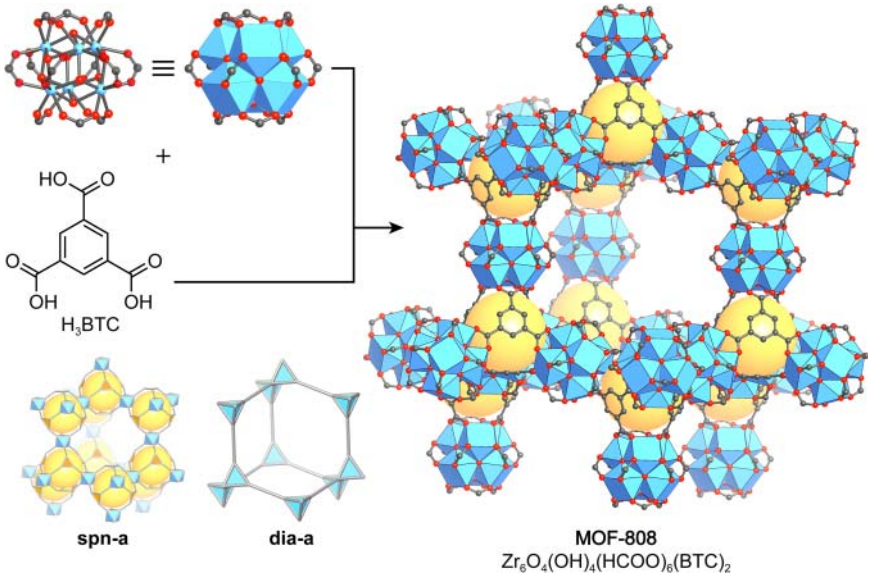

Figure 4.16 Crystal structure of MOF-808. Trigonal antiprismatic zirconium SBUs are linked by trigonal tritopic BTC linkers to form tetrahedral units. These are further connected in a vertex-sharing manner resulting in the formation of adamantine-shaped cages. Thus, the crystal structure of MOF-808 is described by either the **spn** or **dia** net depending on which subunits are chosen as the vertices. The augmented **spn** and **dia** net are depicted in the inset. All hydrogen atoms are omitted for clarity. Color code: Zr, blue; C, gray; O, red.

UMCM-309a the $[Zr_6(\mu_3\text{-}O)_4(\mu_3\text{-}OH)_4]^{12+}$ clusters are connected to six BTB linkers in a hexagonal planar fashion and the remaining uncoordinated metal sites are occupied by six –OH and six $–OH_2$ ligands, resulting in a 6-connected layered structure. It should be noted that these layers can form a 3D interpenetrated structure, which is avoided by using sterically demanding modulators in the synthesis [22]. A comparison of both structures and their underlying topologies is given in Figure 4.17.

4.3 MOFs Built from 7-, 8-, 10-, and 12-Connected SBUs

4.3.1 7-Connected (7-c) SBUs

Building units with a low point group symmetry are rarely used in MOF chemistry. This is due to the fact that the formation of highly symmetric structures is more favorable and such structures are generally easier to crystallize. In Chapter 3, we saw that low symmetry linkers can be used to construct MOFs and, in a similar way, SBUs with low symmetry can yield crystalline frameworks. An example is a MOF constructed from a 7-c zinc-based SBUs – an SBU that is closely related to the well-studied 6-c $Zn_4O(–COO)_6$ SBU – that are linked by tetratopic H4BPTC linkers. Consequently, the framework crystallizes in a previously unreported 4,7-connected net [23].

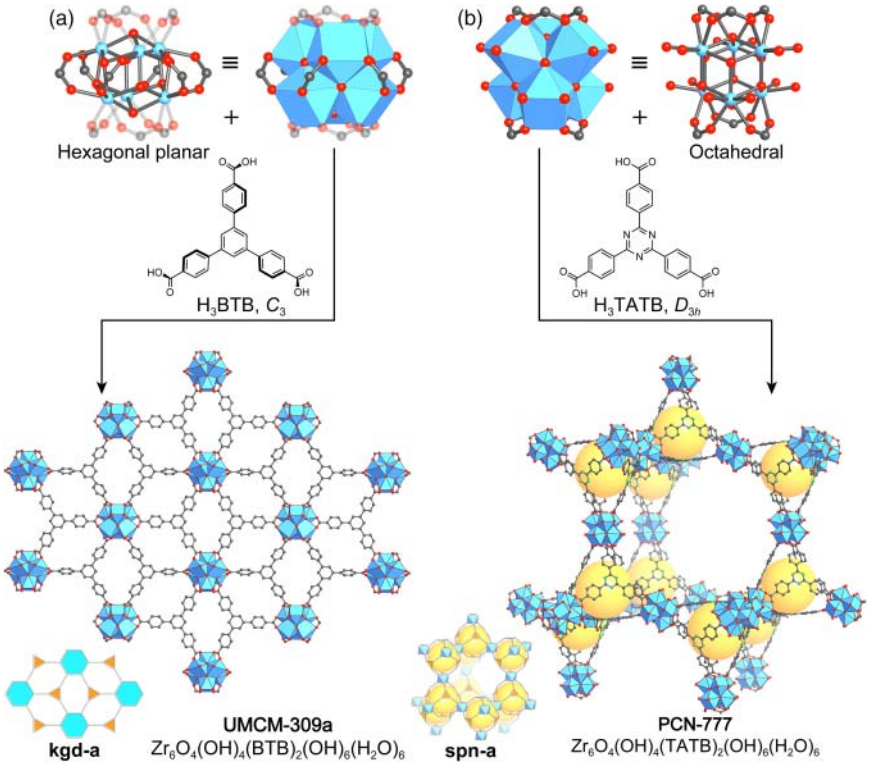

Figure 4.17 Comparison of the crystal structures of UMCM-309a and PCN-777, both built from 6-c zirconium SBUs and trigonal tritopic linkers. The lower symmetry of H_3BTB (C_3) used in the synthesis of UMCM-309a compared to H_3TATB (D_{3h}) directs the reticulation to a (a) **kgd** net rather than (b) an **spn** net. Topology representation of the augmented versions of **kgd** and **spn** are given next to the corresponding structure. All hydrogen atoms are omitted for clarity. Color code: Zr, blue; C, gray; N, green; O, red.

4.3.2 8-Connected (8-c) SBUs

As we will see later in this chapter, most SBUs with a connectivity higher than six are typically based on highly charged metal ions such as Al^{3+}, Cr^{3+}, Ti^{4+}, Zr^{4+}, or Hf^{4+}. There are however rare examples of 8-c SBUs built from divalent metal ions as exemplified by the cubic $Cu_4Cl(-COO)_8$ SBU. Reticulation of these 8-c $Cu_4Cl(-COO)_8$ SBUs and trigonal tritopic H_3BTC linkers yields an anionic **the** framework with chemical formula $(Cu_4Cl_3)(BTC)_8(R_4N)_3$ (R = methyl, ethyl, propyl) (Figure 4.18). Even though the **the** net describes the structure of this MOF accurately, an alternative description based on tetrahedral units can be used to further simplify the structure, in a manner akin to what was described earlier in this chapter for MIL-100 and MIL-101. When each $Cu_4Cl(-COO)_8$ is represented as a 4-membered ring of linked tetrahedra, a **sod** (sodalite) net results. Despite their low surface areas of about 800 $m^2\ g^{-1}$,

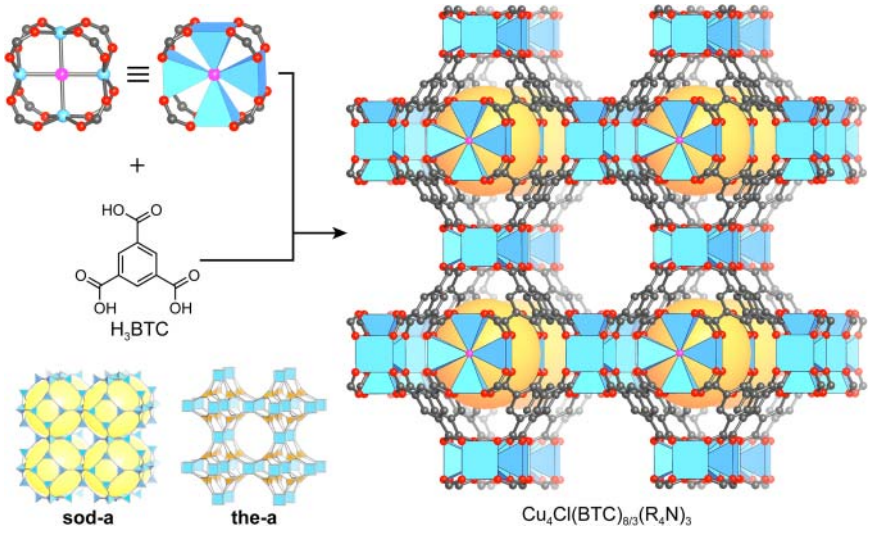

Figure 4.18 Crystal structure of $Cu_4Cl(BTC)_8(R_4N)_3$. The cubic $Cu_4Cl(–COO)_8$ SBUs are joined by tritopic BTC linkers to form cages of **tro** (truncated octahedron, sodalite) topology. The resulting structure is therefore best described by the **sod** rather than the **the** net. The augmented **sod** and **the** net are depicted in the inset. All hydrogen atoms and counter ions residing in the pores are omitted for clarity. Color code: Cu, blue; C, gray; O, red; Cl, pink.

$(Cu_4Cl_3)(BTC)_8(R_4N)_3$ materials have a high sorption capacity for CO_2, which is attributed to the pore partitioning effect of the anionic framework [24].

There are many MOF structures involving 8-c zirconium or hafnium SBUs. Here, we will discuss only selected examples, illustrating the linker-directed synthesis of such frameworks. Linking cubic 8-c SBUs by ditopic linkers can lead to the formation of frameworks with two different topologies: **bcu** (body centered cubic) and **reo** (rhenium oxide). Both can be targeted for MOFs based on Zr_6O_8-core SBUs by adjusting the geometry of the linker. The default topology for linking cubes through ditopic linkers is the **bcu** net (highest symmetry embedding $I\,m\bar{3}m$, No. 229, transitivity 1111), which is expected to form when linear ditopic linkers are reticulated with cubic 8-c SBUs. In contrast, bent linkers are expected to direct the framework formation toward the **reo** topology (highest symmetry embedding $P\,m\bar{3}m$, No. 223, transitivity 1122). Examples for these two cases are PCN-700 ($Zr_6O_4(OH)_4(Me_2\text{-BPDC})_4(OH)_4(H_2O)_4$) and DUT-67 (DUT = Dresden University of Technology, $Zr_6O_6(OH)_2(TDC)_4(CH_3COO)_2$, TDC = thiophene-2,5-dicarboxylic acid), respectively. Both MOFs are synthesized from a Zr^{4+} source that forms cubic 8-c SBUs, and ditopic carboxylate linkers of linear and bent geometry, respectively [25]. The formation of a **bcu** net by linking cubic 8-c Zr_6O_8-core SBUs requires a linear ditopic linker with perpendicular terminal carboxylic acid binding groups (dihedral angle of 90°). Introduction of methyl substituents in the 2- and 2′-position of the planar H_2BPDC linker introduces a twist (rotation around φ) due to steric hindrance (see Figure 4.4). Therefore, the reticulation of $(Me)_2$-BPDC with

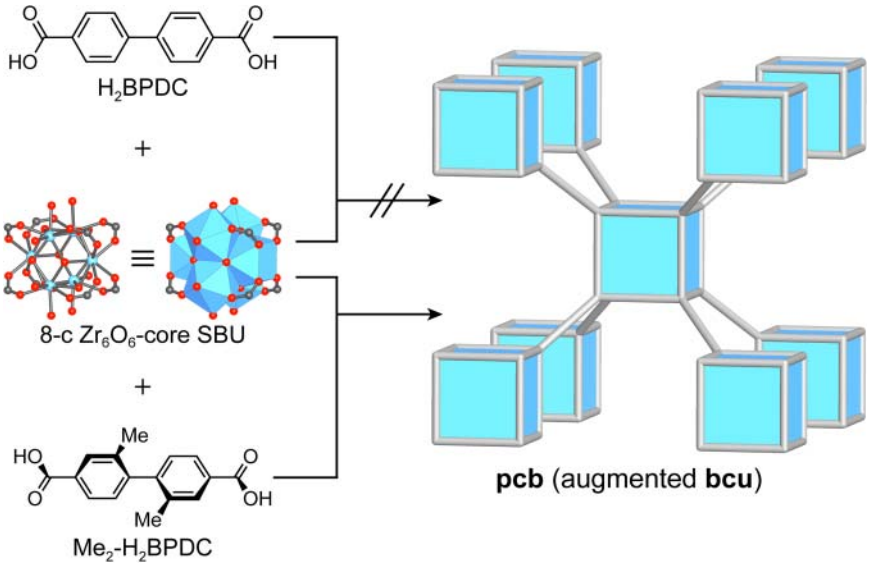

Figure 4.19 Appending methyl substituents in the 2- and 2′-position of the H_2BPDC linker engenders a dihedral angle of 90° between the two binding groups. This geometry is a prerequisite for the formation of a **bcu** net from cubic 8-c zirconium SBUs. The augmented **bcu** net is referred to as the **pcb** (polycubane) net. In contrast, employing unsubstituted H_2BPDC under otherwise identical conditions does not afford a **bcu** framework (see 12-c SBUs). Color code: Zr, blue; C, gray, O, red.

cubic 8-c Zr_6O_8-core SBUs as illustrated in Figure 4.19 yields PCN-700 with the anticipated **bcu** topology.[5]

When ditopic linkers with an angle θ (see Figure 4.4) between coplanar carboxylic acid groups are used, the formation of the default **bcu** topology is avoided, and the formation of **reo** frameworks is favored. This approach is used for the synthesis of DUT-67, which is built from cubic 8-c Zr_6O_8-core SBUs that are joined by bent ditopic TDC linkers featuring an angle of $\theta = 147.9°$ between the coplanar binding groups (Figure 4.20). The synthesis of an isoreticular expanded form of DUT-67 is however challenging because it requires the angle between the two carboxylic acid groups of the linker to remain the same. In H_2DTTDC, fusing three thiophene units results in an angle $\theta = 148.6°$ ($\theta_{(TDC)} = 147.9°$) between the coplanar carboxylic acid groups. At the same time the distance between the two carboxylates is increased by almost 4 Å compared to the parent H_2TDC (Figure 4.20). Using this linker, DUT-51, the isoreticular expanded analog of the **reo** MOF DUT-67, can be prepared.

Figure 4.21 shows a comparison of the structures of PCN-700 and DUT-67. The **bcu** topology is formed with linear ditopic linkers featuring perpendicular binding groups, whereas a framework of **reo** topology results when bent linkers with a precisely adjusted angle θ are used.

5 An isostructural framework with a mixed Zr_6Ni_4 SBU can be prepared by post-synthetic metalation [26].

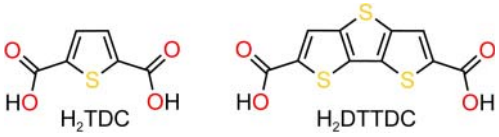

Figure 4.20 Bent ditopic linkers employed in the synthesis of zirconium-based frameworks with **reo** topology. An angle $\theta = 147.9°$ in H_2TDC is required for the formation of **reo** frameworks. Isoreticular expansion requires the angle θ to remain the same, which is achieved by fusing three thiophene units together to give H_2DTTDC ($\theta_{(DTTDC)} = 148.6°$).

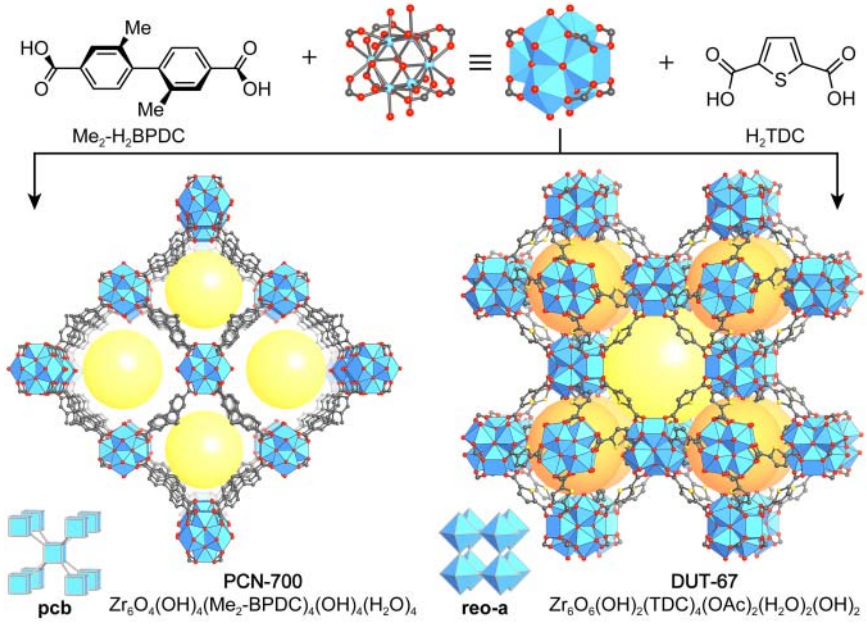

Figure 4.21 Comparison of the crystal structures and topologies of PCN-700 and DUT-67. Both frameworks are built from 8-c zirconium SBUs and ditopic linkers. Employing a linear linker with a dihedral angle $\varphi = 90°$ favors the formation of frameworks of **bcu** topology, whereas the use of a bent linker with an angle θ of around 148° between the coplanar binding groups directs the synthesis toward **reo** topology frameworks. Topology representations of **pcb** and **reo-a** are given next to the corresponding crystal structure. All hydrogen atoms are omitted for clarity. Color code: Zr, blue; C, gray; O, red; S, yellow.

Connecting 8-c Zr_6O_8-core SBUs by tetratopic linkers is expected to give 4,8-connected frameworks with varying topologies. The default net for the combination of cubic 8-c SBUs and tetratopic tetrahedral linkers is the "fluorite" (**flu**) net (e.g. MOF-841), whereas for the combination of cubic 8-c SBUs and tetratopic square linkers three different nets can result: **csq** (e.g. MOF-545), **scu** (e.g. NU-902, NU = Northwestern University), and **sqc** (e.g. PCN-225) [27].[6]

6 The letter "s" and "c" in all three topologies (**csq**, **sqc**, and **scu**) refer to "cube" and "square" and all three nets are referred to as "SC-nets."

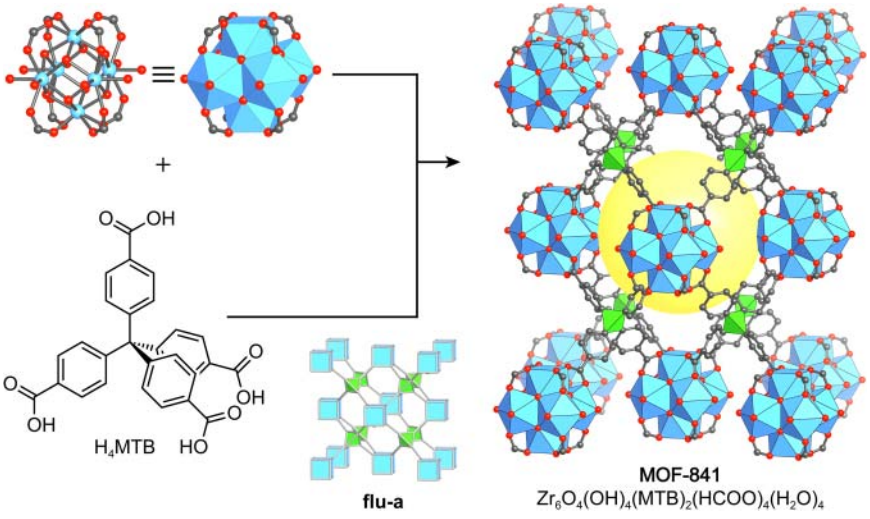

Figure 4.22 Crystal structure of MOF-841. The combination of a tetrahedral linker (H_4MTB) and a cubic 8-c zirconium SBU results in a framework of **flu** topology. Here, the zirconium clusters form a face centered packing while the MTB linkers occupy the tetrahedral holes. The large pore in the center of the unit cell corresponds to the octahedral hole in the structure of CaF_2. The inset shows a topology representation of the augmented **flu** net. All hydrogen atoms are omitted and green tetrahedra are placed at the center of the MTB linkers for clarity. Color code: Zr, blue; C, gray; O, red.

The structure of MOF-841 ($Zr_6O_4(OH)_4(MTB)_2(HCOO)_4(H_2O)_4$) is built from tetrahedral MTB linkers connecting four cubic $Zr_6(\mu_3\text{-}O)_4(\mu_3\text{-}OH)_4(\text{–}COO)_8$ SBUs (Figure 4.22). The combination of cubic and tetrahedral building units gives rise to the highly symmetric default topology (**flu**, edge transitive), which is derived from the structure of the mineral CaF_2 (Fluorite). Consequently, the arrangement of the zirconium SBUs is described as cubic face centered and all tetrahedral holes are filled by MTB linkers. The structure of MOF-841 encompasses one type of pore with a diameter of 11.6 Å that corresponds to the octahedral holes in the fluorite structure [19].

The combination of 8-c cubic SBUs and tetrahedral tetratopic linkers can only result in the formation of the **flu** net. In contrast, when 8-c Zr_6O_8-core SBUs and a tetratopic porphyrin-based linker (H_4TCPP-H_2) are reticulated, frameworks with three different topologies are formed by adjusting the pH, the concentration of the modulator, and the reaction temperature. When considering topological isomers (nets built from identical building units but having different topologies), as a rule of thumb, the isomer having the topology with the most symmetric "highest symmetry embedding" is the thermodynamically favored phase, whereas those with less symmetric highest symmetry embeddings are the kinetic products. This allows us to sort the three possible topologies for the combination of squares and cubes as follows: the **csq** net is the thermodynamic product (highest symmetry embedding $P\,6/mmm$, No. 191, transitivity 2155), whereas the topologies with a less symmetric highest symmetry embedding, namely **sqc** (highest symmetry embedding $P\,4_1/amd$, No. 141, transitivity 2132) and **scu**

(highest symmetry embedding $P\,4/mmm$, No. 123, transitivity 2133) correspond to kinetic products. High reaction temperatures combined with a strongly binding modulator in high concentrations are thus expected to drive the reaction toward the thermodynamically favored frameworks of **csq** topology. In contrast, gradually lowering the strength of the modulator as well as the reaction temperatures will favor the kinetically controlled formation of frameworks with **sqc** and eventually with **scu** topology.

We illustrate this principles with three topological isomers: MOF-545 ($Zr_6O_4(OH)_4(TCPP\text{-}H_2)_2(H_2O)_8$) (**csq**), PCN-225 ($Zr_6O_4(OH)_4(TCPP\text{-}H_2)_2(H_2O)_4(OH)_4$) (**sqc**), and NU-902 ($Zr_6O_4(OH)_4(TCPP\text{-}H_2)_2(H_2O)_4(OH)_4$) (**scu**) [27]. All three MOFs are prepared by reacting a Zr^{4+} salt and $H_4TCPP\text{-}H_2$ in *N*,*N*-dimethylformamide (DMF) or *N*,*N*-diethylformamide (DEF) using the following modulators and temperatures: the addition of formic acid ($pK_a = 3.75$) and a high reaction temperature of 130 °C in DMF gives MOF 545 (**csq**), the addition of benzoic acid ($pK_a = 4.19$) and heating to 120 °C in DEF yields PCN-225 (**sqc**), and the use of acetic acid ($pK_a = 4.75$) combined with a low reaction temperature of 90 °C in DMF affords NU-902 (**scu**). A comparison of the structures of MOF-545, PCN-225, and NU-902 is given in Figure 4.23. It is worth noting that not only the modulator and the temperature influence the formation of a particular phase but also the solvent, especially considering that it is the source of the base released upon decomposition. DMF releases dimethylamine (DMA, $pK_b = 10.7$), whereas DEF releases diethylamine (DEA, $pK_b = 11.1$). DEA is a slightly stronger base than DMA and thus the formation of the kinetic product is more favorable from DEF solutions.

4.3.3 10-Connected (10-c) SBUs

In the discussion of 8-c SBUs we saw that the reticulation of ditopic bent linkers and Zr^{4+} ions results in frameworks of **reo** topology as exemplified by DUT-67. Using the same linker (H_2TDC) employed in the synthesis of DUT-67 and reacting it with a zirconium salt while decreasing the concentration of the modulator (acetic acid) compared to the synthesis conditions of DUT-67 directs the reaction toward the formation of a 10-c zirconium SBU, and consequently a framework of **btc** (body-centered tetragonal) topology, termed DUT-69 ($Zr_6O_4(OH)_4(TDC)_5(CH_3COO)_2$). To rationalize this finding, the role of the modulator in the crystallization of MOFs must be considered in more detail. Monofunctional carboxylic acids compete with the carboxylate-based linkers and thus prevent adjacent SBUs from aggregating into larger fragments by modulating the rate of framework formation. Hence, in MOF synthesis such compounds are referred to as modulators. A higher connectivity of the SBU is observed for lower concentrations or less strongly binding modulators, or higher concentrations of the linker. Such reaction conditions lead to a higher likelihood for open binding sites of the SBU to be occupied by the linker or the more facile replacement of modulator molecules by the linker, respectively. This is indeed the case for DUT-69 where a net with higher connectivity (10-c **bct** net) is formed using starting materials identical to those used to prepare

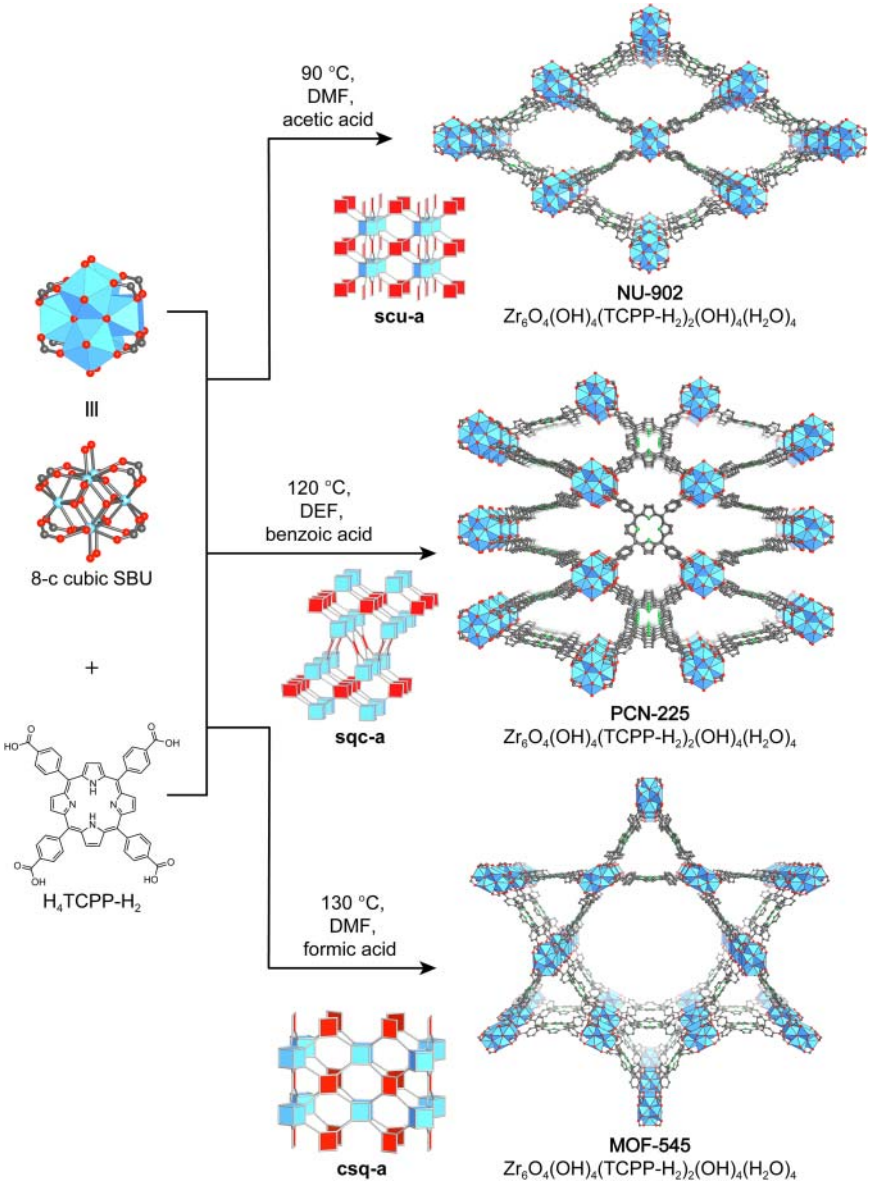

Figure 4.23 Comparison of the crystal structures and topologies of NU-902 (**scu**), PCN-225 (**sqc**), and MOF-545 (**csq**) (top to bottom). The topology with the most symmetric highest symmetry embedding is formed as the thermodynamic product (**csq**, MOF-545). Milder reaction conditions result in the formation of **sqc** (PCN-225) and **scu** (NU-902) nets. Topology representations of **scu**, **sqc**, and **csq** are given next to the corresponding crystal structures. All hydrogen atoms are omitted for clarity. Color code: Zr, blue; C, gray; N, green; O, red.

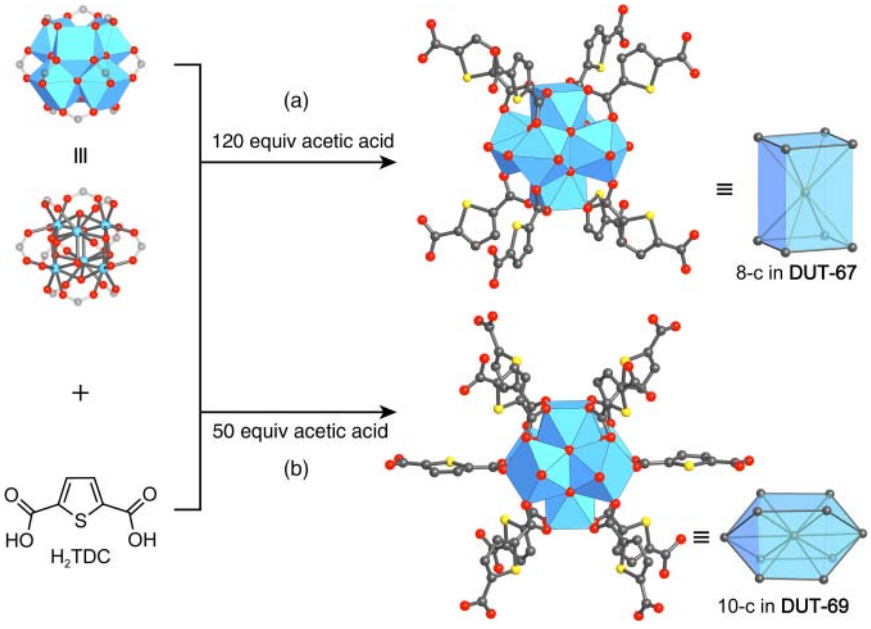

Figure 4.24 Comparison of the SBUs in the structures of (a) DUT-67 (8-c, **reo** net) and (b) DUT-69 (10-c, **bct** net) and their respective vertex figures. A higher connectivity is achieved by lowering the concentration of the modulator under otherwise similar conditions. All hydrogen atoms are omitted for clarity. Color code: Zr, blue; C, gray; O, red; S, yellow.

DUT-67 (8-c **reo** net) but in the presence of a lower concentration of the acetic acid modulator (Figure 4.24).

In the crystal structure of DUT-69 each 10-c Zr_6O_8-core SBU is linked to 10 TDC linkers giving rise to octahedral cages of 5 Å in diameter. Rectangular channels with a pore aperture of 9.15×2.66 Å propagate along the crystallographic *c*-axis. The crystal structure of DUT-69 alongside the corresponding **bct-a** net is shown in Figure 4.25.

4.3.4 12-Connected (12-c) SBUs

Similar to the example described above, the connectivity of the Zr_6O_8-core SBU can be further increased by adjusting the ratio of the metal source and the linker employed in the synthesis. The structures of MOF-841 and MOF-812 ($Zr_6O_4(OH)_4(MTB)_3(H_2O)_2$) are both built from tetrahedral MTB linkers and Zr_6O_8-core SBUs [19]. While MOF-841 crystallizes in the 4,8-connected **flu** net (Figure 4.22), in the case of MOF-812 a 12-connected SBU and consequently a structure with an underlying **ith** (icosahedron-tetrahedron) topology forms (Figure 4.26). This is realized by changing the ratio of starting materials employed in the synthesis. MOF-841 is prepared from a mixture of H_4MTB and zirconyl chloride ($ZrOCl_2$) in a ratio of 1 : 4 whereas the higher connected structure of MOF-812 forms when the relative concentration of the linker is increased (linker to metal ratio is decreased to 1 : 2) under otherwise almost identical conditions [19].

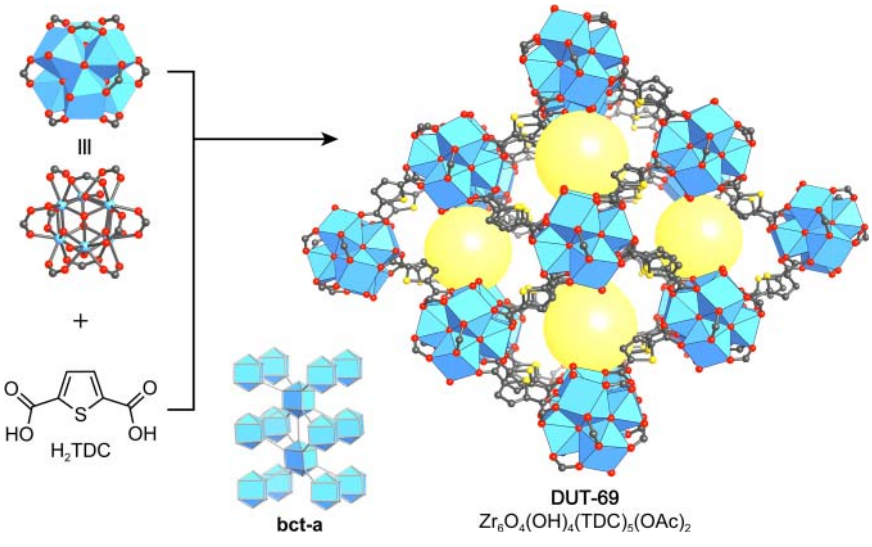

Figure 4.25 Crystal structure of DUT-69 projected along the *c*-direction. 10-c zirconium SBUs are linked by bent TDC linkers to form a 3D framework of **bct** topology with channels of 9.15 × 2.66 Å running along the crystallographic *c*-axis. The topology representation shows the augmented **bct** net viewed along the *a*-direction. All hydrogen atoms are omitted for clarity. Color code: Zr, blue; C, gray; O, red; S, yellow.

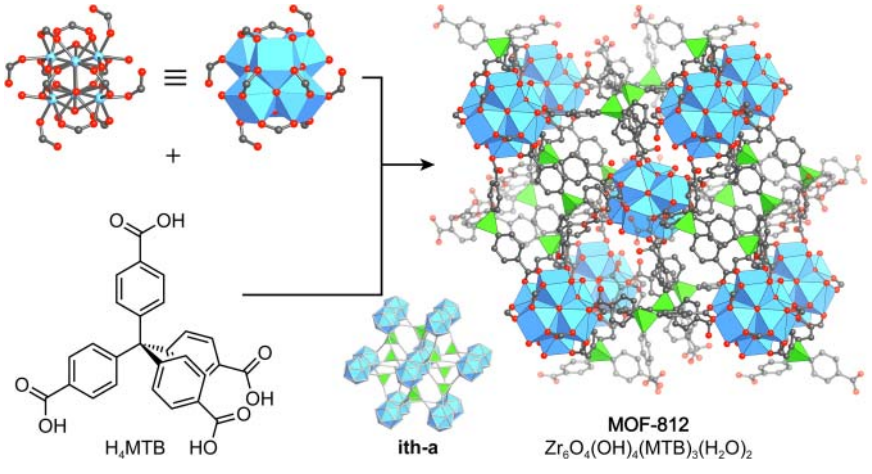

Figure 4.26 The **ith** net of MOF-812 is formed by reticulation of Zr^{4+} and tetrahedral tetratopic H_4MTB linkers. Four MTB linkers are bound to the SBU in a monodentate fashion and eight in a bridging fashion, resulting in an overall "8 + 4-connectivity" of the SBU. The structure has one type of pore with a diameter of 5.6 Å. The inset shows the augmented **ith** net. All hydrogen atoms are omitted and green tetrahedra are placed at the center of the MTB linkers for clarity. Color code: Zr, blue; C, gray; O, red.

The last two examples illustrate the influence of the concentration of the modulator and the ratio of the starting materials on the connectivity of the resulting SBUs and thus the structure of the resulting MOF. When considering nets of identical connectivity that arise from the same set of starting materials (not building units), adjusting the reaction conditions helps to select which of these nets is preferred. To illustrate this, we take a closer look at two 4,12-connected nets that are formed by linking square planar linkers (H_4TCPP-H_2) and 12-c Zr_6O_8-core SBUs. Two geometries exist for a 12-c zirconium SBU: cuboctahedral and hexagonal prismatic. Linking such SBUs with square planar building units leads to the formation of frameworks of **ftw** (e.g. MOF-525, $Zr_6O_4(OH)_4$(TCPP-$H_2)_3$) or **shp** (e.g. PCN-223, $Zr_6O_4(OH)_4$(TCPP-$H_2)_3$) topology, respectively (Figure 4.27). Both are the default topologies for the combination of their respective vertex geometries [27c]. While PCN-223 is formed in the presence of high concentrations of the modulator and at high reaction temperatures (120 °C), MOF-525 forms under milder conditions, meaning a lower concentration of modulator and relatively low reaction temperatures (65 °C). The pores in the cubic **ftw** structure of MOF-525 are surrounded by eight cuboctahedral $Zr_6(\mu_3\text{-}O)_4(\mu_3\text{-}OH)_4(-COO)_{12}$ SBUs and six TCPP-H_2 linkers. In contrast, PCN-223 has trigonal 1D pores and a lower surface area than MOF-525 as a consequence of the closer packing of hexagonal prismatic $Zr_6(\mu_3\text{-}O)_4(\mu_3\text{-}OH)_4(-COO)_{12}$ SBUs in the **shp** net.

The first reported, and still most prominent, 12-c MOF based on zirconium SBUs is UiO-66 (UiO = University of Oslo, $Zr_6O_4(OH)_4(BDC)_{12}$) [28]. UiO-66 crystallizes in in a **fcu** (face-centered cubic) net constructed from cuboctahedral 12-c Zr_6O_8-core SBUs and linear ditopic BDC linkers. The open 3D framework structure encompasses tetrahedral and octahedral pores where each octahedral pore is surrounded by eight tetrahedral ones in a face-sharing manner (Figure 4.28). The highly connected and therefore relatively dense structure is prone to defects in the form of missing linkers or missing SBUs [29]. Hence, UiO-66 was subject to many studies on defects in MOFs and properties resulting from them. All MOFs of the isoreticular series based on UiO-66 feature high architectural and chemical stability.

Zirconium-based MOFs comprise by far the largest fraction of MOFs containing 12-c SBUs. However, it should be noted, that even though they are rare, 12-c SBUs of di- and trivalent metals such as beryllium, aluminum, and chromium, as well as some zinc-based examples exist.

A synthetic strategy of matching the geometry between tetrahedrally coordinated silicon and zinc ions is employed in the synthesis of a framework based on 12-c $Zn_8(SiO_4)(-COO)_{12}$ SBUs. These SBUs are composed of a central tetrahedral SiO_4 unit that is connected to four tetrahedrally coordinated Zn^{2+} ions in a vertex-sharing manner [30]. Connecting the SBUs by 12 BDC linkers that propagate in doubles along six directions results in a double cross-linked interpenetrated 6-c framework ($Zn_8(SiO)_4(BDC)_6$) with an overall **pcu** topology (Figure 4.29). This MOF exhibits outstanding thermal (up to 520 °C) and chemical stability, arguably due to the double cross-linking of the SBUs in combination with framework interpenetration. The 12-c $Zn_8(SiO_4)(-COO)_{12}$ SBU can be used to prepare further frameworks with linkers such as *m*-BDC [31].

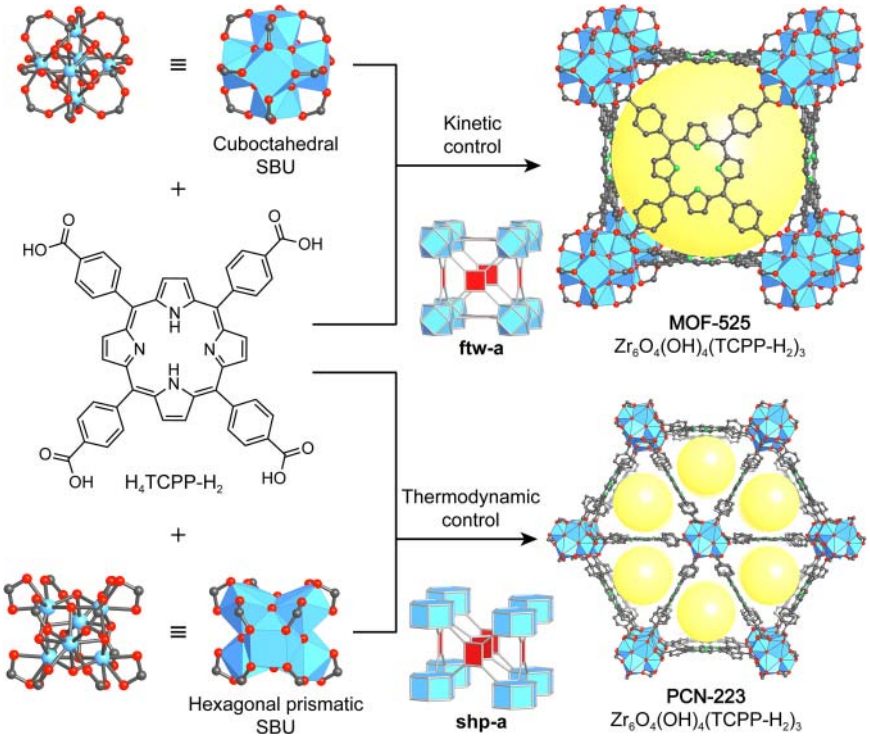

Figure 4.27 Comparison of the crystal structures and underlying topologies of MOF-525 (top) and PCN-223 (bottom). Both structures are based on 4,12-connected nets. The **shp** framework PCN-223 is formed under comparatively harsh conditions, whereas the **ftw** MOF-525 forms under mild reaction conditions. While MOF-525 has discrete cubic pores, PCN-223 has a 1D pore system. The closer packing of hexagonal prismatic SBUs in PCN-223 results in smaller pores and a lower surface area compared to MOF-525. Topology representations of both, **ftw** and **shp**, are given next to the corresponding crystal structures. All hydrogen atoms are omitted for clarity. Color code: Zr, blue; C, gray; N, green; O, red.

A different strategy for making MOFs with unusual 12-c zinc SBUs is used to prepare bio-MOF-100 ($Zn_4O_2(AD)_4(BPDC)_6(Me_2NH_2)_4$) [32]. Its 12-c SBU of chemical formula $Zn_8O_2(AD)_4(-COO)_{12}$ (ZABU) is built from eight tetrahedrally coordinated Zn^{2+} ions and four adeninates (AD). It is terminated by 12 carboxylates of 12 BPDC linkers that are bound to the SBU in a monodentate fashion. The ZABU SBU can be described as a truncated tetrahedron and the framework formed by linking these SBUs with linear ditopic BPDC linkers is a triple cross-linked 4-connected net with overall **lcs** topology (Figure 4.30). The cubic structure of bio-MOF-100 contains only mesopores and activation by supercritical drying yields a highly porous material with an internal surface area of 4300 $m^2\ g^{-1}$ and a free pore volume of about 85%. bio-MOF-100 is an ideal platform for post-synthetic linker exchange reactions, a post-synthetic modification that is discussed in more detail in Chapter 6 [33].

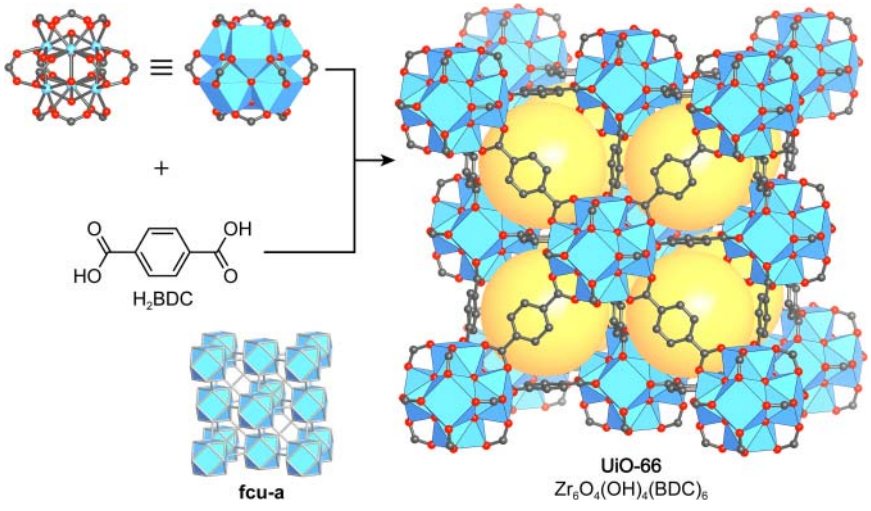

Figure 4.28 Crystal structure and **fcu** topology of UiO-66. 12-c zirconium SBUs are connected by linear ditopic BDC linkers resulting in a face centered arrangement of the SBUs (**fcu** net). The structure has two different pores that are equivalent to the tetrahedral (orange spheres) and octahedral holes (not shown for clarity) in a face-centered cubic arrangement. The inset shows the augmented **fcu** net. All hydrogen atoms are omitted for clarity. Color code: Zr, blue; C, gray; O, red.

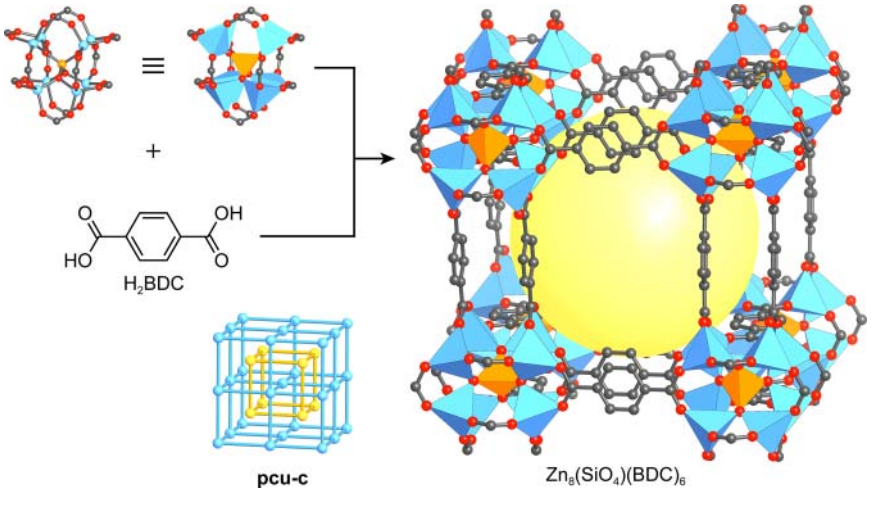

Figure 4.29 Crystal structure of $Zn_8(SiO_4)(BDC)_6$. The 12-c SBUs are connected in six directions in a double cross-linked manner, resulting in a framework of **pcu** topology. The open space encompassed by this framework is partially filled by an interpenetrating framework (catenated, **pcu-c**). The double cross-linking as well as the interpenetration endow $Zn_8(SiO_4)(BDC)_6$ with high thermal stability. All hydrogen atoms are omitted for clarity. Color code: Zn, blue; Si, orange; C, gray; O, red.

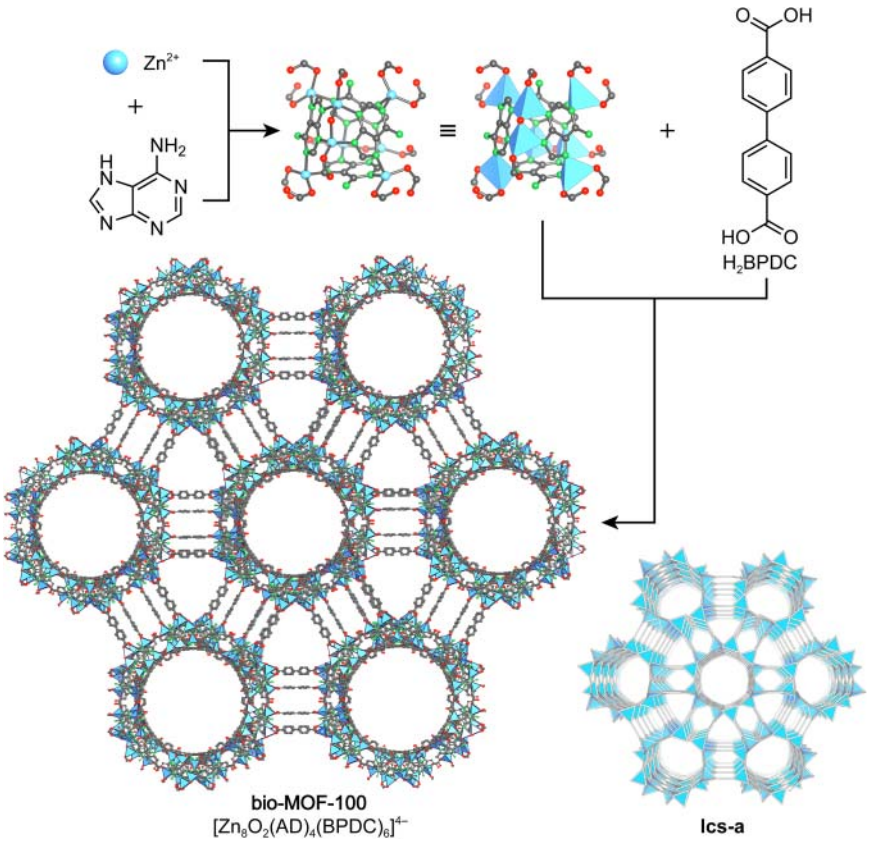

Figure 4.30 Crystal structure of bio-MOF-100. Truncated tetrahedral $Zn_8O_2(AD)_4(–COO)_{12}$ (ZABU) SBUs are triple cross-linked by BPDC resulting in a framework of **lcs** topology. The structure contains only mesopores and has a free pore volume of about 85%.

The development of MOFs constructed from SBUs containing light metals or metalloids is of great interest. To illustrate why, it is instructive to consider the substitution of Zn^{2+} in MOF-5 by the lightest divalent metal in the periodic table, Be^{2+}. This exchange theoretically results in a 40% increase in both gravimetric surface area ($m^2\ g^{-1}$) and gravimetric hydrogen storage capacity ($cm^3\ g^{-1}$) while the high volumetric capacity of MOF-5 is retained [34]. Inspired by this idea, a MOF of formula $Be_{12}(OH)_{12}(BTB)_4$ was synthesized, marking the first structurally characterized beryllium-based MOF [34d]. The highly porous framework structure is built from saddle-shaped $[Be_{12}(OH)_{12}]^{12+}$ SBUs composed of 12 tetrahedrally coordinated Be^{2+} ions. The inside edge of these ring-SBUs is bridged by –OH groups and the periphery is linked by carboxylates of the trigonal BTB linkers connecting the SBUs (Figure 4.31a). The 12-membered ring SBU constitutes a novelty as it was previously unknown in the realm of molecular metal carboxylates. Owing to its low weight, $Be_{12}(OH)_{12}(BTB)_4$ shows a high gravimetric hydrogen storage capacity of 9.2 wt% at 100 bar and 77 K.

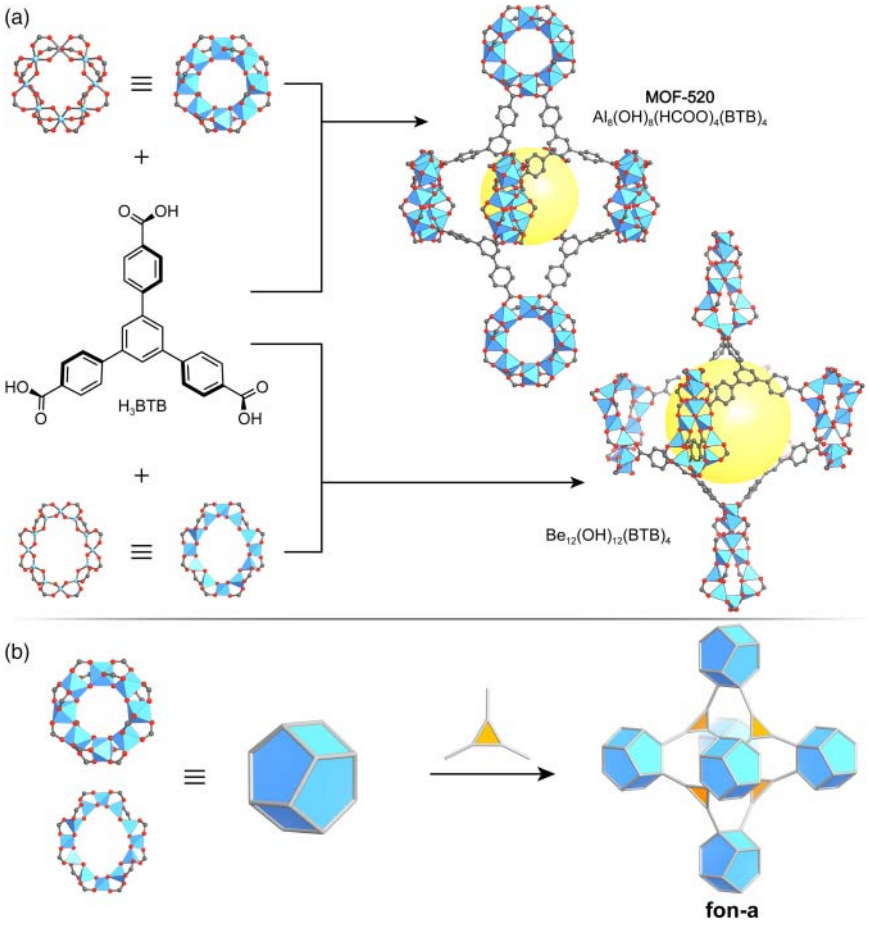

Figure 4.31 (a) Comparison of the crystal structure of MOF-520 (top) and $Be_{12}(OH)_{12}(BTB)_4$ (bottom). Both frameworks have a 3,12-connected **fon** topology. $Be_{12}(OH)_{12}(BTB)_4$ is built from 12-membered –OH bridged saddle-shaped SBUs, whereas the ring-shaped SBUs in MOF-520 consist of eight vertex-sharing hydroxyl bridged aluminum octahedra. (b) Topology representation of MOF-520 and $Be_{12}(OH)_{12}(BTB)_4$. The 12-c SBUs are shown in blue, the tritopic BTB linkers are represented by orange triangles. All hydrogen atoms are omitted for clarity. Color code: Zr, blue; C, gray; O, red.

A similar ring-shaped aluminum-based SBU is found in the structure of MOF-520 ($Al_8(OH)_8(HCOO)_4(BTB)_4$), a framework synthesized by the reticulation of Al^{3+} ions with trigonal tritopic H_3BTB linkers. MOF-520 shares the same topology with the aforementioned $Be_{12}(OH)_{12}(BTB)_4$ [35]. The 3,12-connected **fon** net of MOF-520 is built from octanuclear $Al_8(OH)_8(HCOO)_4(–COO)_{12}$ SBUs consisting of eight octahedrally coordinated vertex-sharing aluminum atoms that are connected by doubly bridging hydroxyl ions (Figure 4.31). Each SBU is connected to 12 BTB linkers and 4 terminal formates, which allows for large pores of 16.2×9.9 Å.

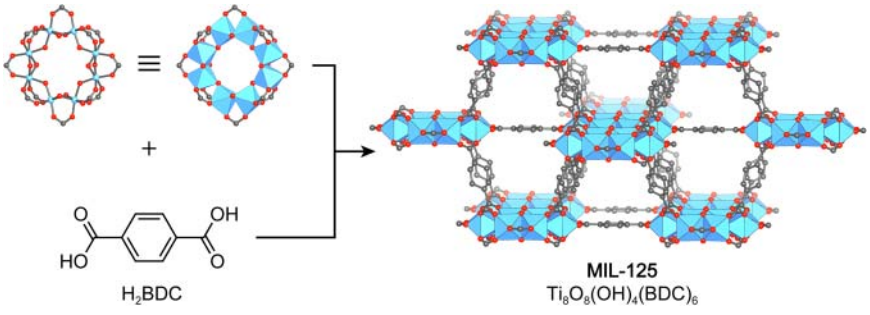

Figure 4.32 Crystal structure of MIL-125. The structure can be described as a body-centered arrangement of ring-shaped $Ti_8O_8(OH)_4(–COO)_{12}$ SBUs connected by linear ditopic BDC linkers. The resulting augmented **bcu** net has two distinct pores corresponding to the tetrahedral and octahedral holes of a body-centered cubic packing. All hydrogen atoms are omitted for clarity. Color code: Ti, blue; C, gray; O, red.

Among all metals employed in the construction of SBUs, titanium is one of the most attractive candidates, largely due to its low toxicity, redox activity, photocatalytic properties, and the high stability of carboxylate-based titanium MOFs. MIL-125 ($Ti_8O_8(OH)_4(BDC)_6$) is the first reported titanium MOF (Figure 4.32) [36]. Its structure is composed of cyclic octamers of corner-sharing $TiO_5(OH)$ octahedra connected by linear ditopic BDC linkers to form a porous structure with an underlying **bcu** topology. The structure can be described as a body-centered cubic arrangement of ring-shaped $Ti_8O_8(OH)_4(–COO)_{12}$ SBUs. Each SBU is connected to 12 neighboring SBUs by 12 BDC linkers, 4 of which are in the plane of the ring-shaped SBU, 4 are above, and 4 below. This arrangement results in two distinct pores with an accessible pore diameter of 6.13 and 12.55 Å that can be thought of as the octahedral and tetrahedral holes in a body-centered cubic packing, respectively [36].

4.4 MOFs Built from Infinite Rod SBUs

So far, we have only discussed discrete 0D SBUs with a defined connectivity; however, 1D SBUs with infinite rod-like structures are also known in MOF chemistry. It is worthwhile noting that such SBUs are not known as isolated molecular entities but are exclusive to MOF chemistry. Even though most MOFs containing rod SBUs are built from rare earth metals, we will focus on materials built from transition metals as we did for the discrete 0D SBUs. For a comprehensive compilation as well as an in-depth discussion of MOFs with rod SBUs including such involving rare earth metals, the reader is referred elsewhere [37].

We already encountered MOFs with rod SBUs in Chapter 2 when we discussed the structure of MOF-74 and its isoreticular expanded analogs. Another important example of a series of MOFs based on rod SBUs is the MIL-53 series (M(BDC)(OH), where M = Cr^{3+}, Fe^{3+}, Al^{3+}, V^{3+}) [38]. The structure of MIL-53 is built from chains of octahedrally coordinated M^{3+} ions connected by BDC

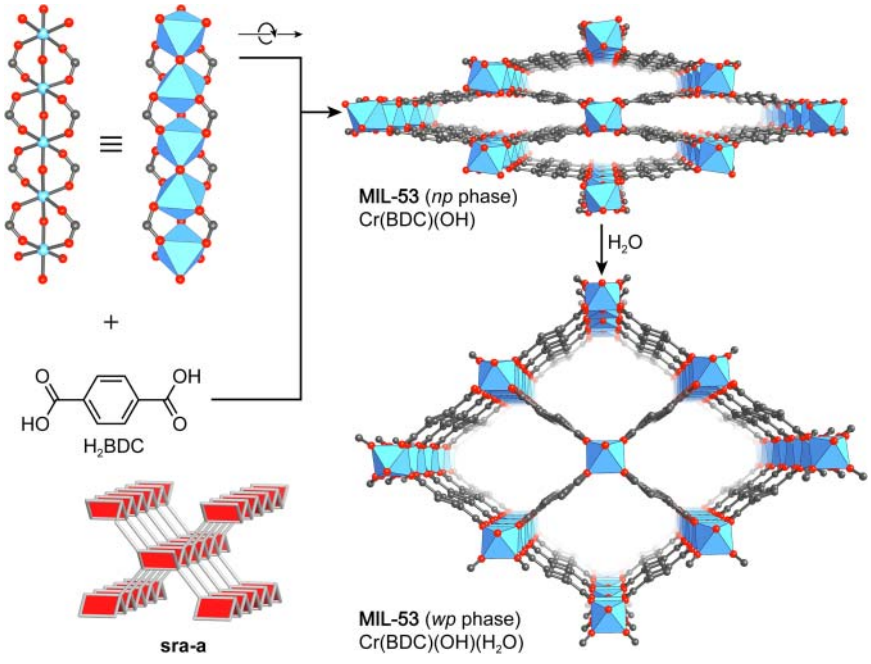

Figure 4.33 Crystal structure of MIL-53, a MOF built from $[Cr(–COO)_{4/4}(OH)_2]_\infty$ rod SBUs linked by linear ditopic BDC linkers to form a framework of **sra** topology. Interaction of the framework with molecular guests possessing large quadrupole or dipole moments results in a breathing motion of the framework. The insert illustrates the augmented **sra** net. All hydrogen atoms are omitted for clarity. Color code: Cr, blue; C, gray; O, red.

linkers to form a 3D microporous structure of **sra** topology with an array of 1D channels running along the crystallographic *c*-axis (Figure 4.33). The rod SBUs are built from $[Cr(–COO)_{4/4}(OH)_{2/2}]$ octahedra where the carboxylates of the two linkers connect two metal centers in a bridging mode. MIL-53 is particularly interesting as an unusual structural distortion upon CO_2 adsorption is observed. A "breathing" motion of the whole framework caused by the quadrupole moment of CO_2 affords a structural transition from its pristine narrow pore (*np*) geometry into an open wide pore (*wp*) phase [39]. This phenomenon was also studied in the presence of other gases with large dipole or quadrupole moments such as water where a similar deformation of the structure is observed.

Rod SBUs can also be of a helical shape. An illustrative example for this is the helical rod SBU in the structure of a chiral MOF of formula $Ni_{2.5}(OH)(L\text{-}Asp)_2$ [40]. The structure of this framework is composed of helical $[M_4(OH)_2(–COO)_2]_\infty$ rod SBUs and $[Ni(L\text{-}Asp)_2]^{2-}$ metallo-linkers. The helical SBUs in this chiral MOF of **srs** topology are built from edge- and corner-sharing Ni octahedra and are all of the same hand. Linking these helices leads to the formation of chiral helical channels of 5×8 Å running along the crystallographic *c*-axis (Figure 4.34).

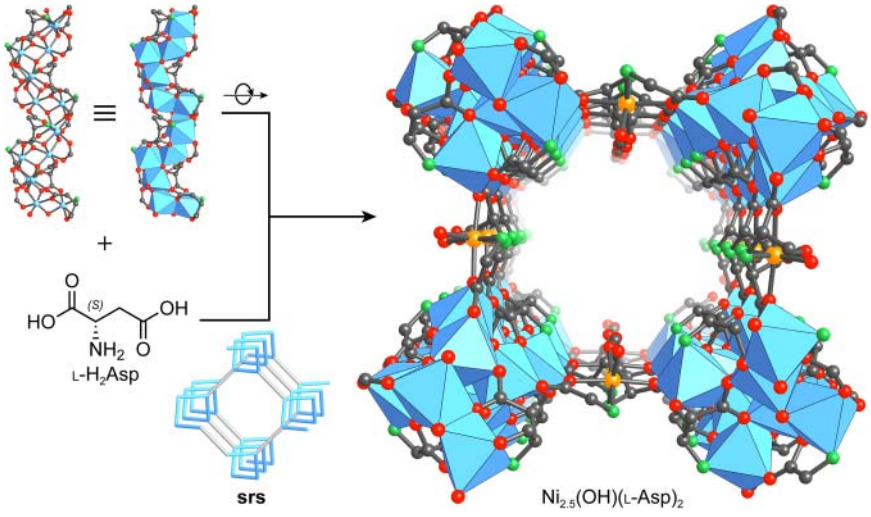

Figure 4.34 Crystal structure of $Ni_{2.5}(OH)(L\text{-}Asp)_2$, a framework built from 1D helical SBUs linked into an **srs** topology by linear $[Ni(L\text{-}Asp)_2]^{2-}$ metallo-linkers. The augmented **srs** net is depicted in the insert. All hydrogen atoms are omitted for clarity. Color code: Ni within the SBU, blue; Ni within the metallo-linker, orange; C, gray; N, green; O, red.

4.5 Summary

In this chapter we discussed the structures of MOFs built from discrete SBUs with a connectivity ranging from 3 to 12 as well as those of frameworks built from rod-like SBUs. We showed that in many cases the precise local geometry of the linker and the SBU, their chemical nature, and the reaction conditions strongly influence the structure of the resulting framework. A classification of structures built from building units of identical local symmetry into thermodynamic and kinetic products was introduced and we showed that this distinction can be made based on the analysis of the corresponding network topology. We provided a general understanding of why specific structures form and how they can be targeted by careful analysis of the requirements to their building units and adjustment of the reaction conditions. All structures discussed in this chapter are built from one type of SBU and one type of linker. It is however possible to synthesize MOFs that combine three or more distinct building units within one structure, and these will be the subject of Chapter 5.

References

1 Grzesiak, A.L., Uribe, F.J., Ockwig, N.W. et al. (2006). Polymer-induced heteronucleation for the discovery of new extended solids. *Angewandte Chemie International Edition* 45 (16): 2553–2556.

2 (a) Han, L., Xu, L.-P., and Zhao, W.-N. (2011). A novel 2D (3,5)-connected coordination framework with $Zn_2(COO)_3$ SBU. *Journal of Molecular Structure*

1000 (1–3): 58–61. (b) Wu, M., Jiang, F., Wei, W. et al. (2009). A porous polyhedral metal-organic framework based on $Zn_2(COO)_3$ and $Zn_2(COO)_4$ SBUs. *Crystal Growth & Design* 9 (6): 2559–2561. (c) Zhang, X., Zhang, Y.-Z., Zhang, D.-S. et al. (2015). A hydrothermally stable Zn(II)-based metal-organic framework: structural modulation and gas adsorption. *Dalton Transactions* 44 (35): 15697–15702. (d) Yang, J., Wang, X., Dai, F. et al. (2014). Improving the porosity and catalytic capacity of a zinc paddlewheel metal-organic framework (MOF) through metal-ion metathesis in a single-crystal-to-single-crystal fashion. *Inorganic Chemistry* 53 (19): 10649–10653.

3 Eddaoudi, M., Kim, J., Wachter, J. et al. (2001). Porous metal-organic polyhedra: 25 Å cuboctahedron constructed from 12 $Cu_2(CO_2)_4$ paddle-wheel building blocks. *Journal of the American Chemical Society* 123 (18): 4368–4369.

4 Furukawa, H., Kim, J., Ockwig, N.W. et al. (2008). Control of vertex geometry, structure dimensionality, functionality, and pore metrics in the reticular synthesis of crystalline metal-organic frameworks and polyhedra. *Journal of the American Chemical Society* 130 (35): 11650–11661.

5 Eddaoudi, M., Kim, J., Vodak, D. et al. (2002). Geometric requirements and examples of important structures in the assembly of square building blocks. *Proceedings of the National Academy of Sciences* 99 (8): 4900–4904.

6 Eddaoudi, M., Kim, J., O'Keeffe, M., and Yaghi, O.M. (2002). $Cu_2[o\text{-Br-}C_6H_3(CO_2)_2]_2(H_2O)_2(DMF)_8(H_2O)_2$: a framework deliberately designed to have the NbO structure type. *Journal of the American Chemical Society* 124 (3): 376–377.

7 Yaghi, O.M., O'Keeffe, M., Ockwig, N.W. et al. (2003). Reticular synthesis and the design of new materials. *Nature* 423 (6941): 705–714.

8 Chui, S.S.-Y., Lo, S.M.-F., Charmant, J.P.H. et al. (1999). A chemically functionalizable nanoporous material $[Cu_3(TMA)_2(H_2O)_3]_n$. *Science* 283 (5405): 1148–1150.

9 (a) Millward, A.R. and Yaghi, O.M. (2005). Metal-organic frameworks with exceptionally high capacity for storage of carbon dioxide at room temperature. *Journal of the American Chemical Society* 127 (51): 17998–17999. (b) Mason, J.A., Veenstra, M., and Long, J.R. (2014). Evaluating metal-organic frameworks for natural gas storage. *Chemical Science* 5 (1): 32–51.

10 Feldblyum, J.I., Liu, M., Gidley, D.W., and Matzger, A.J. (2011). Reconciling the discrepancies between crystallographic porosity and guest access as exemplified by Zn-HKUST-1. *Journal of the American Chemical Society* 133 (45): 18257–18263.

11 (a) Spanopoulos, I., Tsangarakis, C., Klontzas, E. et al. (2016). Reticular synthesis of HKUST-like tbo-MOFs with enhanced CH_4 storage. *Journal of the American Chemical Society* 138 (5): 1568–1574. (b) Ma, S., Sun, D., Ambrogio, M. et al. (2007). Framework-catenation isomerism in metal-organic frameworks and its impact on hydrogen uptake. *Journal of the American Chemical Society* 129 (7): 1858–1859. (c) Furukawa, H., Go, Y.B., Ko, N. et al. (2011). Isoreticular expansion of metal-organic frameworks with triangular and square building units and the lowest calculated density for porous crystals. *Inorganic Chemistry* 50 (18): 9147–9152.

12 Chen, B., Eddaoudi, M., Hyde, S. et al. (2001). Interwoven metal-organic framework on a periodic minimal surface with extra-large pores. *Science* 291 (5506): 1021–1023.
13 Sun, D., Ma, S., Ke, Y. et al. (2006). An interweaving MOF with high hydrogen uptake. *Journal of the American Chemical Society* 128 (12): 3896–3897.
14 (a) Sudik, A.C., Côté, A.P., and Yaghi, O.M. (2005). Metal-organic frameworks based on trigonal prismatic building blocks and the new "acs" topology. *Inorganic Chemistry* 44 (9): 2998–3000. (b) Férey, G., Serre, C., Mellot-Draznieks, C. et al. (2004). A hybrid solid with giant pores prepared by a combination of targeted chemistry, simulation, and powder diffraction. *Angewandte Chemie* 116 (46): 6456–6461. (c) Férey, G., Mellot-Draznieks, C., Serre, C., and Millange, F. (2005). Crystallized frameworks with giant pores: are there limits to the possible? *Accounts of Chemical Research* 38 (4): 217–225. (d) Férey, G., Mellot-Draznieks, C., Serre, C. et al. (2005). A chromium terephthalate-based solid with unusually large pore volumes and surface area. *Science* 309 (5743): 2040–2042. (e) Hong, D.-Y., Hwang, Y.K., Serre, C. et al. (2009). Porous chromium terephthalate MIL-101 with coordinatively unsaturated sites: surface functionalization, encapsulation, sorption and catalysis. *Advanced Functional Materials* 19 (10): 1537–1552. (f) Liu, Y., Eubank, J.F., Cairns, A.J. et al. (2007). Assembly of metal-organic frameworks (MOFs) based on indium-trimer building blocks: a porous MOF with soc topology and high hydrogen storage. *Angewandte Chemie International Edition* 46 (18): 3278–3283. (g) Alezi, D., Belmabkhout, Y., Suyetin, M. et al. (2015). MOF crystal chemistry paving the way to gas storage needs: aluminum-based soc-MOF for CH_4, O_2, and CO_2 storage. *Journal of the American Chemical Society* 137 (41): 13308–13318.
15 Eddaoudi, M., Sava, D.F., Eubank, J.F. et al. (2015). Zeolite-like metal-organic frameworks (ZMOFs): design, synthesis, and properties. *Chemical Society Reviews* 44 (1): 228–249.
16 Bromberg, L., Diao, Y., Wu, H. et al. (2012). Chromium(III) terephthalate metal organic framework (MIL-101): HF-free synthesis, structure, polyoxometalate composites, and catalytic properties. *Chemistry of Materials* 24 (9): 1664–1675.
17 (a) Horcajada, P., Chevreau, H., Heurtaux, D. et al. (2014). Extended and functionalized porous iron(III) tri-or dicarboxylates with MIL-100/101 topologies. *Chemical Communications* 50 (52): 6872–6874. (b) Feng, D., Liu, T.-F., Su, J. et al. (2015). Stable metal-organic frameworks containing single-molecule traps for enzyme encapsulation. *Nature Communications* 6: 5979.
18 Kickelbick, G. and Schubert, U. (1997). Oxozirconium methacrylate clusters: $Zr_6(OH)_4O_4(OMc)_{12}$ and $Zr_4O_2(OMc)_{12}$ (OMc = methacrylate). *European Journal of Inorganic Chemistry* 130 (4): 473–478.
19 Furukawa, H., Gándara, F., Zhang, Y.-B. et al. (2014). Water adsorption in porous metal-organic frameworks and related materials. *Journal of the American Chemical Society* 136 (11): 4369–4381.

20 Feng, D., Wang, K., Su, J. et al. (2015). A highly stable zeotype mesoporous zirconium metal-organic framework with ultralarge pores. *Angewandte Chemie International Edition* 54 (1): 149–154.

21 Ma, J., Wong-Foy, A.G., and Matzger, A.J. (2015). The role of modulators in controlling layer spacings in a tritopic linker based zirconium 2D microporous coordination polymer. *Inorganic Chemistry* 54 (10): 4591–4593.

22 Wang, R., Wang, Z., Xu, Y. et al. (2014). Porous zirconium metal-organic framework constructed from 2D → 3D interpenetration based on a 3,6-connected kgd net. *Inorganic Chemistry* 53 (14): 7086–7088.

23 Bai, S., Zhang, W., Ling, Y. et al. (2015). Predicting and creating 7-connected Zn_4O vertices for the construction of an exceptional metal-organic framework with nanoscale cages. *CrystEngComm* 17 (9): 1923–1926.

24 Tan, Y.-X., He, Y.-P., and Zhang, J. (2011). Pore partition effect on gas sorption properties of an anionic metal-organic framework with exposed Cu^{2+} coordination sites. *Chemical Communications* 47 (38): 10647–10649.

25 (a) Yuan, S., Lu, W., Chen, Y.-P. et al. (2015). Sequential linker installation: precise placement of functional groups in multivariate metal-organic frameworks. *Journal of the American Chemical Society* 137 (9): 3177–3180. (b) Bon, V., Senkovskyy, V., Senkovska, I., and Kaskel, S. (2012). Zr(IV) and Hf(IV) based metal-organic frameworks with reo-topology. *Chemical Communications* 48 (67): 8407–8409.

26 Yuan, S., Chen, Y.P., Qin, J. et al. (2015). Cooperative cluster metalation and ligand migration in zirconium metal-organic frameworks. *Angewandte Chemie International Edition* 54 (49): 14696–14700.

27 (a) Jiang, H.-L., Feng, D., Wang, K. et al. (2013). An exceptionally stable, porphyrinic Zr metal-organic framework exhibiting pH-dependent fluorescence. *Journal of the American Chemical Society* 135 (37): 13934–13938. (b) Deria, P., Gómez-Gualdrón, D.A., Hod, I. et al. (2016). Framework-topology-dependent catalytic activity of zirconium-based (porphinato) zinc(II) MOFs. *Journal of the American Chemical Society* 138 (43): 14449–14457. (c) Morris, W., Volosskiy, B., Demir, S. et al. (2012). Synthesis, structure, and metalation of two new highly porous zirconium metal-organic frameworks. *Inorganic Chemistry* 51 (12): 6443–6445.

28 (a) Cavka, J.H., Jakobsen, S., Olsbye, U. et al. (2008). A new zirconium inorganic building brick forming metal organic frameworks with exceptional stability. *Journal of the American Chemical Society* 130 (42): 13850–13851. (b) Feng, D., Gu, Z.-Y., Chen, Y.-P. et al. (2014). A highly stable porphyrinic zirconium metal-organic framework with shp-a topology. *Journal of the American Chemical Society* 136 (51): 17714–17717.

29 Trickett, C.A., Gagnon, K.J., Lee, S. et al. (2015). Definitive molecular level characterization of defects in UiO-66 crystals. *Angewandte Chemie International Edition* 54 (38): 11162–11167.

30 Yang, S., Long, L., Jiang, Y. et al. (2002). An exceptionally stable metal-organic framework constructed from the $Zn_8(SiO_4)$ core. *Chemistry of Materials* 14 (8): 3229–3231.

31 Yang, S., Long, L., Huang, R., and Zheng, L. (2002). $[Zn_8(SiO_4)(C_8H_4O_4)_6]_n$: the firstborn of a metallosilicate-organic hybrid material family ($C_8H_4O_4$ = isophthalate). *Chemical Communications* (5): 472–473.

32 An, J., Farha, O.K., Hupp, J.T. et al. (2012). Metal-adeninate vertices for the construction of an exceptionally porous metal-organic framework. *Nature Communications* 3: 604.

33 Li, T., Kozlowski, M.T., Doud, E.A. et al. (2013). Stepwise ligand exchange for the preparation of a family of mesoporous MOFs. *Journal of the American Chemical Society* 135 (32): 11688–11691.

34 (a) Bragg, W. (1923). Crystal structure of basic beryllium acetate. *Nature* 111: 532. (b) Pauling, L. and Sherman, J. (1934). The structure of the carboxyl group II. The crystal structure of basic beryllium acetate. *Proceedings of the National Academy of Sciences* 20 (6): 340–345. (c) Han, S.S., Deng, W.-Q., and Goddard, W.A. (2007). Improved designs of metal-organic frameworks for hydrogen storage. *Angewandte Chemie International Edition* 46 (33): 6289–6292. (d) Sumida, K., Hill, M.R., Horike, S. et al. (2009). Synthesis and hydrogen storage properties of $Be_{12}(OH)_{12}$(1,3,5-benzenetribenzoate)$_4$. *Journal of the American Chemical Society* 131 (42): 15120–15121.

35 Gándara, F., Furukawa, H., Lee, S., and Yaghi, O.M. (2014). High methane storage capacity in aluminum metal-organic frameworks. *Journal of the American Chemical Society* 136 (14): 5271–5274.

36 Dan-Hardi, M., Serre, C., Frot, T. et al. (2009). A new photoactive crystalline highly porous titanium(IV) dicarboxylate. *Journal of the American Chemical Society* 131 (31): 10857–10859.

37 (a) Schoedel, A., Li, M., Li, D. et al. (2016). Structures of metal-organic frameworks with rod secondary building units. *Chemical Reviews* 116 (19): 12466–12535. (b) Rosi, N.L., Kim, J., Eddaoudi, M. et al. (2005). Rod packings and metal-organic frameworks constructed from rod-shaped secondary building units. *Journal of the American Chemical Society* 127 (5): 1504–1518. (c) Cheng, P. and Bosch, M. (2015). *Lanthanide Metal-Organic Frameworks*. Springer.

38 (a) Millange, F., Serre, C., and Ferey, G. (2002). Synthesis, structure determination and properties of MIL-53as and MIL-53ht: the first Cr^{III} hybrid inorganic–organic microporous solids: $Cr^{III}(OH)\cdot\{O_2C–C_6H_4–CO_2\}\cdot\{HO_2C–C_6H_4–CO_2H\}_x$. *Chemical Communications* (8): 822–823. (b) Serre, C., Millange, F., Thouvenot, C. et al. (2002). Very large breathing effect in the first nanoporous chromium(III)-based solids: MIL-53 or $Cr^{III}(OH)\cdot\{O_2C–C_6H_4–CO_2\}\cdot\{HO_2C–C_6H_4–CO_2H\}_x\cdot H_2O_y$. *Journal of the American Chemical Society* 124 (45): 13519–13526. (c) Loiseau, T., Serre, C., Huguenard, C. et al. (2004). A rationale for the large breathing of the porous aluminum terephthalate (MIL-53) upon hydration. *Chemistry – A European Journal* 10 (6): 1373–1382.

39 Boutin, A., Coudert, F.-X., Springuel-Huet, M.-A. et al. (2010). The behavior of flexible MIL-53(Al) upon CH_4 and CO_2 adsorption. *The Journal of Physical Chemistry C* 114 (50): 22237–22244.

40 Anokhina, E.V., Go, Y.B., Lee, Y. et al. (2006). Chiral three-dimensional microporous nickel aspartate with extended Ni–O–Ni bonding. *Journal of the American Chemical Society* 128 (30): 9957–9962.